Decreased mitochondrial respiration in aneurysmal aortas of Fibulin-4 mutant mice is linked to PGC1A regulation

Pluijm, I. van der; Burger, J.; Heijningen, P.M. van; Ijpma, A.; Vliet, N. van; Milanese, C.; ... ; Essers, J.

ESC European Society of Cardiology

Cardiovascular Research (2018) **114**, 1776–1793
doi:10.1093/cvr/cvy150

Decreased mitochondrial respiration in aneurysmal aortas of Fibulin-4 mutant mice is linked to PGC1A regulation

Ingrid van der Pluijm[1,2]*, Joyce Burger[2,3¶], Paula M. van Heijningen[2¶], Arne IJpma[4], Nicole van Vliet[2], Chiara Milanese[2], Kees Schoonderwoerd[3], Willem Sluiter[2], Lea-Jeanne Ringuette[5], Dirk H. W. Dekkers[6], Ivo Que[7], Erik L. Kaijzel[7], Luuk te Riet[1,8], Elena G. MacFarlane[9], Devashish Das[2†], Reinier van der Linden[10‡], Marcel Vermeij[11], Jeroen A. Demmers[6], Pier G. Mastroberardino[2], Elaine C. Davis[5], Hiromi Yanagisawa[12], Harry C. Dietz[9,13,14], Roland Kanaar[15,16], and Jeroen Essers[1,15,16]*

[1]Department of Vascular Surgery, Erasmus MC, Wytemaweg 80, 3015 CN Rotterdam, The Netherlands; [2]Department of Molecular Genetics, Erasmus MC, Wytemaweg 80, 3015 CN Rotterdam, The Netherlands; [3]Department of Clinical Genetics, Erasmus MC, Wytemaweg 80, 3015 CN Rotterdam, The Netherlands; [4]Clinical Bioinformatics Unit, Department of Pathology, Erasmus MC, Wytemaweg 80, 3015 CN Rotterdam, The Netherlands; [5]Department of Anatomy and Cell Biology, McGill University, 3640 Rue University, Montréal, QC H3A 0C7, Canada; [6]Proteomics Center, Erasmus MC, Wytemaweg 80, 3015 CN Rotterdam, The Netherlands; [7]Department of Radiology, Leiden University Medical Center, Albinusdreef 2, 2333 ZA Leiden, The Netherlands; [8]Department of Pharmacology, Erasmus MC, Wytemaweg 80, 3015 CN Rotterdam, The Netherlands; [9]Department of Surgery, McKusick-Nathans Institute of Genetic Medicine, Johns Hopkins University School of Medicine, 733 N Broadway, Baltimore, MD 21205, USA; [10]Stem cell Institute, Erasmus MC, Wytemaweg 80, 3015 CN Rotterdam, The Netherlands; [11]Department of Pathology, Erasmus MC, Wytemaweg 80, 3015 CN Rotterdam, The Netherlands; [12]Life Science Center, Tsukuba Advanced Research Alliance, University of Tsukuba, 1-1-1 Tennodai, Tsukuba, Ibaraki, 305-8577 Japan; [13]Institute of Genetic Medicine, Johns Hopkins University School of Medicine, 733 N Broadway, Baltimore, MD 21205, USA; [14]Division of Pediatric Cardiology, Department of Pediatrics, and Department of Medicine, Johns Hopkins University School of Medicine, 733 N Broadway, Baltimore, MD 21205, USA; [15]Department of Radiation Oncology, Erasmus MC, Wytemaweg 80, 3015 CN Rotterdam, The Netherlands; and [16]Department of Molecular Genetics, Oncode Institute, Erasmus MC, Rotterdan, The Netherlands

Received 7 July 2017; revised 26 September 2017; editorial decision 7 June 2018; accepted 19 June 2018; online publish-ahead-of-print 21 June 2018

Time for primary review: 86 days

Aim Thoracic aortic aneurysms are a life-threatening condition often diagnosed too late. To discover novel robust biomarkers, we aimed to better understand the molecular mechanisms underlying aneurysm formation.

Methods and results In Fibulin-4$^{R/R}$ mice, the extracellular matrix protein Fibulin-4 is 4-fold reduced, resulting in progressive ascending aneurysm formation and early death around 3 months of age. We performed proteomics and genomics studies on Fibulin-4$^{R/R}$ mouse aortas. Intriguingly, we observed alterations in mitochondrial protein composition in Fibulin-4$^{R/R}$ aortas. Consistently, functional studies in Fibulin-4$^{R/R}$ vascular smooth muscle cells (VSMCs) revealed lower oxygen consumption rates, but increased acidification rates. Yet, mitochondria in Fibulin-4$^{R/R}$ VSMCs showed no aberrant cytoplasmic localization. We found similar reduced mitochondrial respiration in Tgfbr-1$^{M318R/+}$ VSMCs, a mouse model for Loeys-Dietz syndrome (LDS). Interestingly, also human fibroblasts from Marfan (FBN1) and LDS (TGFBR2 and SMAD3) patients showed lower oxygen consumption. While individual mitochondrial Complexes I–V activities were unaltered in Fibulin-4$^{R/R}$ heart and muscle, these tissues showed similar decreased oxygen consumption. Furthermore, aortas of aneurysmal Fibulin-4$^{R/R}$ mice displayed increased reactive oxygen species (ROS) levels. Consistent with these findings, gene expression analyses revealed dysregulation of metabolic pathways. Accordingly, blood ketone levels of Fibulin-4$^{R/R}$ mice were reduced and liver fatty acids were decreased, while liver glycogen was increased, indicating dysregulated metabolism at the organismal level. As predicted by gene expression analysis, the activity of PGC1α, a key regulator between mitochondrial function

* Corresponding authors. Tel: +31 10 7043724; fax: +31 10 7044743, E-mail: i.vanderpluijm@erasmusmc.nl (I.v.d.P.); Tel: +31 10 7043604; fax: +31 10 7044743, E-mail: j.essers@erasmusmc.nl (J.E.)

† Present address. Pre-Clinical MRI Facility, Faculty of Science, The University of Sheffield, Western Bank, Sheffield, S10 2TN, UK.

‡ Present address: Department of Quantitative biology, Hubrecht Institute, Utrecht, The Netherlands. www.hubrecht.eu

¶ These authors contributed equally to the study.

and organismal metabolism, was downregulated in Fibulin-4$^{R/R}$ VSMCs. Increased TGFβ reduced PGC1α levels, indicating involvement of TGFβ signalling in PGC1α regulation. Activation of PGC1α restored the decreased oxygen consumption in Fibulin-4$^{R/R}$ VSMCs and improved their reduced growth potential, emphasizing the importance of this key regulator.

Conclusion Our data indicate altered mitochondrial function and metabolic dysregulation, leading to increased ROS levels and altered energy production, as a novel mechanism, which may contribute to thoracic aortic aneurysm formation.

Keywords Aneurysm • Mitochondria • Molecular biology • Organismal metabolism

1. Introduction

Disorders of the heart and blood vessels, together known as cardiovascular disease (CVD), are a leading cause of death. Most often patients present with symptoms at a late and irreversible stage. A striking example is aneurysmal disease, of which the incidence increases with age. Aneurysms are large dilatations of the aorta that, when not detected in time, will result in aortic rupture associated with high mortality. This dilation of the aorta frequently occurs unnoticed up to a point where surgery is the only optional treatment left. Although most risk factors, such as lifestyle and age are known, the molecular mechanisms involved are often not yet fully understood. Without this knowledge, proper diagnosis and intervention treatments are difficult to implement.

The most important factors known to be involved to date are extracellular matrix (ECM) degeneration and alterations in the renin–angiotensin system (RAS) and transforming growth factor β (TGFβ) signalling pathways.[1–8] In fact, intervention strategies based on these targets are being explored.[9] Although some mitigating effects on degeneration and dilatation of the aorta have been observed, none of these treatments rescue the disease or reverse symptoms.[10–12] This must mean that still many processes and molecules involved need to be identified to complete the picture of how aneurysms are formed and progress.

To study the molecular mechanisms that underlie aneurysm formation, we developed a Fibulin-4 mouse model.[13–15] Fibulin-4 is a secreted glycoprotein, which is expressed in medial layers of blood vessels and is a critical component for the structural integrity and elasticity of the aortic wall.[16–18] Fibulin-4 protein levels in the aorta are essential for vascular maturation. The protein is located in microfibril bundles which tether elastic fibres to smooth muscle cells via integrin-mediated binding to regions of the cell membrane that are occupied by intracellular membrane-associated anchoring sites for actin filaments.[19] Insufficient levels of Fibulin-4 compromise the structural integrity of the aortic wall, which can lead to aneurysm formation. In agreement, patients with mutations in Fibulin-4 suffer from cardiovascular complications including aortic aneurysms, arterial tortuosity, and elastin abnormalities.[20–22]

Fibulin-4 is an essential gene and complete deletion of this gene in the mouse leads to perinatal lethality.[23] However, in our Fibulin-4$^{R/R}$ mouse model, Fibulin-4 is 4-fold reduced[13], resulting in severe aortic aneurysms with associated aortic valve disease, thereby closely mimicking aneurysm formation of genetically affected patients. Notably, genome-wide aorta transcriptome and histological analyses of young Fibulin-4$^{R/R}$ animals revealed TGFβ signalling as one of the critical events in the pathogenesis of the observed aneurysm formation.[13]

In this study, in order to identify additional underlying molecular mechanisms that may contribute to aneurysm formation, we performed proteomics, genomics, and functional experiments on aortas of adult Fibulin-4$^{R/R}$ animals. Mostly, proteomics data reports on the absence or presence of certain proteins, whereas gene expression profiling data are subjected to pathway analysis. We hypothesized that by performing pathway analysis on our proteomics data, and by comparing gene and protein expression, this would hint us towards new important pathways that additionally play a role in aneurysm formation. Our omics data point to the fact that altered mitochondrial function and metabolism accompany aneurysm formation in Fibulin-4$^{R/R}$ mice, which we substantiate with functional experiments. These findings offer new mechanistic insights into the complex disease of aneurysm formation.

2. Methods

2.1 Experimental animals

Fibulin-4$^{+/R}$ animals were bred into in a C57BL6 background to obtain Fibulin-4$^{R/R}$ and wild-type mouse (Fibulin-4$^{+/+}$) experimental animals (backcross 7). Fibulin-4^{SMKO} animals, with deletion of Fibulin-4 in VSMCs specifically, were kindly provided by Hiromi Yanigasawa[24] and bred into the same C57BL6 background. The numbers of animals used for each experiment are described in the Results section and mentioned in figures and/or figure legends. For each experiment with mutant animals, littermate controls were used unless stated otherwise. Animals were housed at the Animal Resource Centre (Erasmus University Medical Centre), which operates in compliance with the 'Animal Welfare Act' of the Dutch government, using the 'Guide for the Care and Use of Laboratory Animals' as its standard. As required by Dutch law, formal permission to generate and use genetically modified animals was obtained from the responsible local and national authorities. An independent Animal Ethics Committee consulted by Erasmus Medical Center (Stichting DEC Consult) approved these studies (permit number 140-12-05), in accordance with national and international guidelines. For the described experiments animals were sacrificed by CO_2 inhalation, unless stated otherwise. This study conforms to the guidelines from Directive 2010/63/EU of the European Parliament on the protection of animals used for scientific purposes or the NIH guidelines.

2.2. Preparation of aorta protein extracts and MS/MS protein identification

Fibulin-4$^{R/R}$ and Fibulin-4$^{+/+}$ littermate control mice ($n = 2$ per group, female) were sacrificed at an age of 80–90 days, and thoracic aortas were collected. Next, aorta protein extracts were made and protein concentration was determined as described.[25] Equal amounts of total protein were loaded and size separated on a gradient (5–20%) SDS gel. Subsequently, gels were stained with Coomassie Brilliant Blue. Lanes were excised from the gel and 5 mm slices were subjected to destaining, in-gel reduction with dithiothreitol, alkylation with chloroacetamide and digestion with trypsin (Promega, sequencing grade), essentially as described.[26] For Nanoflow LC-MS/MS details see Supplementary material online. The analysis was performed in duplicate on independent samples ($n = 2$ per genotype). Proteins with a Mascot score of 60 and higher with

Table 1 Primer sequences used for real-time PCR

	Fw seq	Rev seq	Size
PPARα	AACATCGAGTGTCGAATATGTGG	CCGAATAGTTCGCCGAAAGAA	99
PPARγ	CACAATGCCATCAGGTTTGG	GCTGGTCGATATCACTGGAGATC	82
PGC1α	CTGCGGGATGATGGAGACAG	TCGTTCGACCTGCGTAAAGT	101
PGC1β	GGGAAAAGGCCATCGGTGAA	CAGCACCTGGCACTCTACAA	122
B2M	CTCACACTGAATTCACCCCCA	GTCTCGATCCCAGTAGACGGT	98

a unique peptide count of at least 1, were taken into account for both genotypes separately. To perform an Ingenuity Pathway Analysis (IPA), lists of proteins identified in Fibulin-$4^{R/R}$ and Fibulin-$4^{+/+}$ aortas were aligned and assessed for proteins only present in one or the other, or both. Next, proteins only present in Fibulin-$4^{R/R}$ aortas were designated 'up'. Likewise, proteins only present in Fibulin-$4^{+/+}$ aortas, thus absent in Fibulin-$4^{R/R}$ were designated 'down'. Also, for enrichment of the IPA analysis, we took into account proteins present in both genotypes; proteins with a unique peptide count either two-fold higher or two-fold lower in Fibulin-$4^{R/R}$ compared to Fibulin-$4^{+/+}$ were designated 'up' and 'down', respectively. For proper IPA analysis, arbitrary signs of +2 and -2 were given to a protein designated up or down, respectively. A total of 374 proteins were fed into IPA (80 down, 294 up; also see Supplementary material online, *Tables S1* and *S2*).

2.3 GO-term analysis

To classify proteins according to gene ontology (GO) terms, we used the AgBAse GOretriever for GO-term retrieval, which classifies proteins on the basis of cellular components (http://agbase.msstate.edu/cgi-bin/tools/goretriever_select.pl). For the 374 proteins that were identified as different between Fibulin-$4^{R/R}$ and Fibulin-$4^{+/+}$, 342 could be assigned with a GO-term. These were separated into 12 categories: nucleus, cytoplasm, cytoskeleton, ECM, mitochondrion, proteasome, plasma membrane, ribosomes, endoplasmatic reticulum and sarcoplasmic reticulum (ER and SR), golgi and other (includes all other cellular components not mentioned before), and unknown. For each category, percentages were calculated by dividing proteins present in such category by all proteins assigned with a GO-term.

2.4 Microarray experiments

Total thoracic aorta RNA of 3-month old Fibulin-$4^{+/+}$ (n = 3) and Fibulin-$4^{R/R}$ (n = 2) was obtained using standard procedures (Qiagen). Labelling, hybridization, and scanning of Affymetrix Mouse Exon 1.0 ST microarrays (Affymetrix, Mountain View, CA, USA) were performed according to standard Affymetrix protocol (http://www.affymetrix.com/support/technical/byproduct.affx? product=moexon-st). Raw intensity values of all samples were normalized by robust multichip analysis normalization (background correction and quantile normalization) using Partek version 6.5 (Partek Inc., St. Louis, MO, USA). Principal component analysis showed good separation of the two sample sets. Differential expressed genes were identified using ANOVA (Partek). Cut-off values for significantly expressed genes: *P*-value ≤0.03 and -1.5 ≤ fold change ≥ +1.5. Functional analysis was performed using IPA (Ingenuity, Redwood City, CA, USA). Upstream regulators were selected by *P*-value <0.01, Bias-corrected z-score >2 and <-2. For the comparison of adult and newborn Fibulin-$4^{R/R}$ gene expression data, we used the Fibulin-$4^{R/R}$ newborn data previously published by Hanada *et al.*[13] This comparison resulted in 106 overlapping, significantly regulated genes (FC > 1.2; $P < 0.05$), of which 99 were regulated in the same direction. These 106 overlapping genes were used for pathway analysis in IPA. For upstream regulator analysis the same selection criteria were used as mentioned above.

2.5 RNA isolation and real-time PCR

Liver and aortic tissue from Fibulin-$4^{+/+}$ and Fibulin-$4^{R/R}$ mice, snap frozen and stored at -80°C, was used for this experiment. RNA from aortic tissue was isolated with the miRNeasy mini kit (Qiagen) and liver RNA with RNeasy mini kit (Qiagen). cDNA was made with iScript cDNA synthesis kit (Biorad) according to manufacturing protocol. Q-PCR was performed with 200 nM forward and reverse primers and iQ™ SYBR® Green Supermix (biorad) on the CFX96 system (Biorad); denaturation at 95°C for 3 min, 40 cycles denaturation at 95°C for 15 s, annealing/extension at 55°C for 30 s. B2M was used as a housekeeping gene. Relative gene expression levels were determined with the comparative Ct method. See *Table 1* for primers used.

2.6 Cell culture

Mice (aged 100 days) were euthanized by an overdose of CO_2 and autopsied according to standard protocols. Primary vascular smooth muscle cells (VSMCs) were isolated according to the method of Proudfoot and Shanahan,[27] from the thoracic aorta of Fibulin-$4^{+/+}$, Fibulin-$4^{R/R}$, and Fibulin-4^{SMKO} mice and cultured on gelatinized dishes in Dulbecco's Modified Eagle's Medium (DMEM) (Lonza BioWhittaker) supplemented with 1% penicillin–streptomycin (PS) and 10% foetal calf serum (FCS). Tgfbr-$1^{M318R/+}$ and control VSMCs were kindly provided by Hal Dietz and Elena MacFarlane.[28] VSMCs were used until passage 10 for experiments described unless stated otherwise. Human patient fibroblasts with Fibrillin-1 (FBN1 c.4817-1G>A: FBN1 ex 39), TGFβ receptor 2 (TGFBR2 c.1573delA: TGFBR2 ex 07) and Smad3 (SMAD3 c.859C>T, p.R287W: SMAD3 ex 9) mutations were kindly provide by D.F. Majoor-Krakauer, I.B.M.H. van der Laar, and J.M.A. Verhagen. All patients provided written informed consent for participation in the study, and this study conforms to the principles outlined in the Declaration of Helsinki.

For the proliferation assay, cells were used at passages 7 and 8. Fibulin-$4^{+/+}$ and Fibulin-$4^{R/R}$ VSMCs were seeded in triplicate in 6 cm dishes (5000 cells/dish) and allowed to attach. Cells were fixed overnight at 4°C with 10% trichloroacetic acid (TCA, Sigma-Aldrich, T9159) at Days 1, 2, 3, 6, and 7 after seeding. A sulforhodamine beta (SRB) assay for proliferation was performed after collection of all time points. The fixed and dried dishes were incubated for 20 min with 0.5% SRB solution (Sigma-Aldrich, S9012) in 1% acetic acid and excess SRB was removed by washing with 1% acetic acid. After drying, bound SRB was dissolved in 10 mM TRIS (Sigma-Aldrich, T6066). Absorbance was measured at 560 nm, and the percentage of growth was calculated at each day relative to the number of cells at Day 1.

2.7 Mitochondrial respiration

Oxygen consumption rates (OCR) and extracellular acidification rate (ECAR) were measured using an XF-24 Extracellular Flux Analyzer (Seahorse Bioscience). Respiration was measured in XF assay media (non-buffered DMEM containing 2 mM L-glutamine, 100 mM sodium pyruvate, and 5 mM glucose), in basal conditions and in response to 1 μM oligomycin (ATP synthase inhibitor), 1 μM fluorocarbonyl cyanide phenylhydrazone (FCCP, uncoupler), 1 μM rotenone (Complex I inhibitor), 1 μM antimycin A (Complex III inhibitor). VSMCs and mouse embryonic fibroblasts (MEFs) were seeded at a density of 30 000 cells/well and analysed after 24 h. Optimal cell densities were determined experimentally to ensure a proportional response to FCCP with cell number. ECAR was measured during the entire experiment. For these experiments three independent cell lines were used per genotype, for which 6–8 wells were measured per time point.

2.8 Oxygraph and mitochondrial complex activity measurements

Tissue homogenates were prepared from frozen muscle in 0.25 M sucrose, 10 mM *N*-[2-hydroxyethyl] piperazine-*N*′-[2 ethylsulfonic acid] (HEPES) and 1 mM ethylene diamine tetra-acetic Acid (EDTA), pH 7.4. Mitochondrial respiratory activity, measured as OCR (flux in pmol O_2/s/mg mitochondrial protein) was assessed at 37°C by high-resolution respirometry (Oxygraph-2k, Oroboros Instruments). Complexes I- and II-dependent respiration were measured in state 2 (respectively, in the presence of 2 mmol/L malate and 10 mmol/L glutamate, and in the presence of 10 mmol/L succinate) and state 3 (in the presence of substrates and 0.25 mmol/L ADP). To prevent retrograde flux of electrons via Complex I, Complex II-dependent respiration was measured in the presence of 0.5 μmol/L of the Complex I inhibitor rotenone. Respiratory adenylate control index (RCI) was calculated by dividing oxygen flux in state 3 by the flux in state 2. For complex activity measurements, see Supplementary material online.

2.9 Registration of reactive oxygen species with molecular imaging

Mice were anaesthetized (isoflurane 2%, O_2 2 L/min) and visualized using the IVIS spectrum imaging system (Perkin Elmer). L-012 (8-amino-4-chloro-7-phenylpyridol[3,4-d]pyridazine-1, 4(2*H*, 3*H*)dione, a chemitransluminescent probe and derivative of luminol, was purchased from Wako Chemical (Neuss, Germany) and dissolved in H_2O. A concentration of 75 mg/kg in a volume of 100 μL was administered intravenously. Images were taken with the IVIS Spectrum imaging system (Perkin Elmer). For molecular imaging, mice were sacrificed after an hour by an overdose of anaesthesia, and the chest was opened according to standard necropsy protocols. Data acquisition and analysis were performed using IVIS imaging software Living Image (Caliper). The photon flux was quantified within a region of interest encompassing the thoracic chest region of each mouse. The signal was normalized against an illumination profile for the selected field of view. Also see reference. [29]

2.10 DHE staining

Cryosections 10 μm thick were stored at -80°C. After thawing the sections, they were stained by 5 μM dihydroethidium (DHE) and 0.5 μg/mL Hoechst 33258 in phosphate buffered saline (PBS) for 30 min at 37°C in a humidified atmosphere. The fluorescence of the superoxide specific reaction product of DHE oxidation was measured using a fluorescence inverted microscope (Olympus IX50) equipped with a 460–490 nm band pass excitation filter and 515 nm emission IF-barrier filter, digitized with an F-view camera (Soft Imaging System, Münster, Germany), and analysed offline (AnalySIS 3.1; Soft Imaging System). To determine the integrated density ratio, we first determined the sum of the fluorescence values of the pixels in the ethidium (red) and 2-OH-ethidium (green) selection separately. Subsequently, the integrated intensity ratio was determined by dividing the 2-OH-ethidium (green) values over the ethidium (red) values for the individual samples.

2.11 PGC1α luciferase assay

Fibulin-$4^{+/+}$ and Fibulin-$4^{R/R}$ VSMCs were transiently transfected using lipofectamine 2000 (Invitrogen). Cells were dually transfected with PGC1α 2 kb firefly luciferase plasmid (Addgene plasmid 8887[30]) and SV40-renilla luciferase plasmid (10:1). After 24 h, cells were washed with PBS, replenished with medium containing low serum (0.2% FCS) and cells were either treated overnight with TGFβ1 (5 ng/mL, Biovision) to stimulate TGFβ signalling, SB431542 hydrate (10 μM, Sigma), inhibitor of the TGFβ receptor, Forskolin (10 μM, Sigma) for PGC1α activation, or DMSO as a negative control. After 24 h, cells were lysed and firefly/renilla luciferase ratio was determined with the dual-luciferase assay system (Promega) using Glomax- multi+ detection (Promega) for each cell line. Relative luciferase levels were calculated by using the untreated Fibulin-$4^{+/+}$ VSMCs (control) as reference value.

2.12 Statistical analysis

All experiments described were performed blinded by using cell line and mouse numbers without genotypes. Normal distribution of the data was assessed using the Shapiro Wilk test. The unpaired two-tailed Student's *t*-test was performed to analyse the specific sample groups for significant differences. All results are expressed as mean ± SEM. However, for data with non-normal distribution, log-transformation of the data, followed by the Student's *t*-test, was performed. A *P*-value <0.05 was considered to indicate a significant difference between groups. In the figures, $P < 0.05$ or $P < 0.01$ is shown with * and $P < 0.001$ with **. All analyses were performed using IBM SPSS Statistics version 21.0 (SPSS Inc., Chicago, IL, USA) or Graphpad.

3. Results

3.1 Proteomics analysis identifies increased mitochondrial protein levels in Fibulin-$4^{R/R}$ aortas

For the proteomics analysis, protein extracts isolated from 3-month old thoracic aortas of Fibulin-$4^{R/R}$ and Fibulin-$4^{+/+}$ animals were used. Reduction of Fibulin-4 protein was confirmed by western blot (Supplementary material online, *Figure S1A*, left panel). Proteome expression profiles were analysed using a 1D gradient gel of total aorta protein extract. Next, proteins separated on the gel were trypsin digested and identified by an MS/MS method coupled to Mascot database searches (Supplementary material online, *Table S1*). A duplicate analysis of the samples identified more than 75% of the proteins in the first analysis. Analysis of an independent set of aorta extracts identified more than 65% of the previously identified proteins.

To determine differences in the proteome of Fibulin-$4^{R/R}$ and Fibulin-$4^{+/+}$ aortas, we used a Mascot score cut-off of 60. This resulted in a total of 695 proteins, of which 494 identified proteins for Fibulin-$4^{+/+}$ and 655 identified proteins for Fibulin-$4^{R/R}$ aorta. IPA was performed on a selection of proteins that were either present or absent, as well as proteins

with a two-fold higher or lower peptide count, in Fibulin-4$^{R/R}$ vs. Fibulin-4$^{+/+}$ aorta, designated over- and under-represented, respectively. This resulted in 80 proteins that were over-represented in Fibulin-4$^{+/+}$ compared to Fibulin-4$^{R/R}$ aorta and 294 proteins that were over-represented in Fibulin-4$^{R/R}$ compared to Fibulin-4$^{+/+}$, leaving 321 proteins designated as 'not changed' between Fibulin-4$^{+/+}$ and Fibulin-4$^{R/R}$ (Supplementary material online, *Table S2* and *Figure 1A*).

To verify this approach, we subsequently checked whether we could find proteins known to be associated with aneurysm formation based on three important associated factors: the ECM, TGFβ, and RAS signalling. We used the AgBAse GOretriever for GO-term retrieval, which classifies proteins on the basis of cellular components (http://agbase.msstate.edu/cgi-bin/tools/goretriever_select.pl). Of the 374 proteins in total that were differentially expressed between Fibulin-4$^{R/R}$ and wild-type mice, 342 GO-terms could be assigned. Here, we observed that 14% of these proteins fell into the category 'ECM' (*Figure 1B*). Moreover, compared to wild-type, in the Fibulin-4$^{R/R}$ aorta we observed over-representation of the ECM proteins elastin, fibrillin, fibronectin, laminin, and different collagen subtypes. We performed confocal 3D imaging on aortic walls of Fibulin-4$^{+/+}$ and Fibulin-4$^{R/R}$ mice, showing expanded and disorganized elastin structure in the latter (Supplementary material online, *Figure S1B*). In addition, western blot analysis showed increased amounts of elastin protein in Fibulin-4$^{R/R}$ compared to Fibulin-4$^{+/+}$ aortic extracts (Supplementary material online, *Figure S1C*). Both results confirm the over-representation of the ECM proteins that we observed in proteomics data. Next to this overabundance of ECM proteins, 17% of the proteins fell into the category 'cytoskeleton'. Cytoskeleton proteins are closely connected to the ECM via integrins. Unexpectedly, we also observed that 17% of all proteins with significantly changed expression fell into the category 'mitochondria' (*Figure 1B*).

Next, the 374 deregulated proteins were loaded into IPA for further analysis. Of these 374 protein IDs, 369 were mapped by IPA. We performed both a pathway and an upstream regulator analysis to get an idea of the changes in processes involved. TGFβ1 itself turned out to be upregulated and was also predicted to be activated (based on 69 deregulated target molecules) as part of the upstream regulator analysis (*Figure 1C*). Thus, the proteomics data points to involvement of TGFβ signalling in Fibulin-4 associated aneurysms as previously reported.[13,22,31] Both ACE as well as Rac1, which are part of the RAS pathway, were upregulated in the protein dataset of Fibulin-4$^{R/R}$ compared to Fibulin-4$^{+/+}$. Moreover, angiotensinogen, a key molecule in the RAS pathway, was predicted to be upregulated (*Figure 1C*). Indeed, previous analysis of mouse aortas showed that angiotensinogen is increased in Fibulin-4$^{R/R}$ animals compared to Fibulin-4$^{+/+}$.[5,7] In conclusion, our proteome analysis reveals deregulation of TGFβ signalling and RAS, processes already known to be changed in Fibulin-4$^{R/R}$ aneurysms, validating our approach.

Canonical pathway analysis (IPA) pointed towards changes in cytoskeleton and integrin signalling (*Figure 1D*), as did the GO-analysis, which fits with Fibulin-4's functions within the ECM. Interestingly, mitochondrial dysfunction was also a significantly changed canonical pathway, which fits with the findings of the GO analysis showing a protein over-representation in the category 'mitochondria'. Taken together, next to factors known to be changed in aneurysm formation, our proteomics data analysis suggests changes in mitochondrial function in the aortas of Fibulin-4$^{R/R}$ animals.

3.2 Decreased OCR in mutant Fibulin-4 and TGFβ-1 receptor VSMCs

To investigate mitochondrial function, we analysed mitochondrial respiration using a Seahorse XF-24 Extracellular Flux Analyzer, which allows simultaneous measurement of the OCR and the ECAR. While OCR indicates respiration, ECAR reflects lactate production and thus glycolytic flux. OCR and ECAR thus provide a comprehensive estimate of the bioenergetics properties of the studied specimen. We observed a significantly decreased basal respiration (without addition of any inhibitor) in Fibulin-4$^{R/R}$ VSMCs compared to Fibulin-4$^{+/+}$ controls (*Figure 2A,B*, Phase I, $P < 0.01$). While no differences were observed in respiration after injection of the ATP synthase inhibitor oligomycin, the addition of FCCP, an oxidative phosphorylation (OXPHOS) uncoupler eliciting maximal respiration, indicated a significantly lower maximal OCR in Fibulin-4$^{R/R}$ VSMCs (*Figure 2A,B*, Phase III, $P < 0.01$). Complete repression of respiration by the combined addition of Complex I inhibitor rotenone and Complex III inhibitor antimycin A, led to the same OCR in Fibulin-4$^{R/R}$ and Fibulin-4$^{+/+}$ VSMCs, indicating that besides mitochondrial respiration, oxygen consumption differences due to other cellular processes are negligible (*Figure 2A*). Experiments were repeated three times with two independent cell lines per genotype which gave similar consistent results (*Figure 2B*). Interestingly, ECAR was consistently higher in Fibulin-4$^{R/R}$ compared to Fibulin-4$^{+/+}$ VSMCs (*Figure 2C,D*, $P < 0.01$), which might be indicative of metabolic rearrangements to compensate for mitochondrial defects in Fibulin-4$^{R/R}$ cells. Interestingly, lower basal and maximum OCR were also observed in MEFs of Fibulin-4$^{R/R}$ mice compared to Fibulin-4$^{+/+}$ control mice, highlighting that decreased oxygen consumption is a general phenomenon in the Fibulin-4 $^{R/R}$ mouse model (Supplementary material online, *Figure S2*, $P < 0.01$).

We next wanted to verify that the observed defect in mitochondrial function is due to reduced Fibulin-4 in Fibulin-4$^{R/R}$ cells, rather than potential secondary effects associated with the engineered allele. To this end, we isolated Fibulin-4^{SMKO} VSMCs from the Fibulin-4^{SMKO} mouse, in which Fibulin-4 is knocked out in the smooth muscle cells specifically. Absence of Fibulin-4 in Fibulin-4^{SMKO} aortic extracts was verified by western blot (Supplementary material online, *Figure S1A* right panel). We then performed the same Seahorse experiments as described above for the Fibulin-4$^{R/R}$ VSMCs. Interestingly, also these Fibulin-4^{SMKO} VSMCs showed a significant reduction in both basal and maximal OCR compared to Fibulin-4$^{+/+}$ VSMCs (*Figure 2E*, $P < 0.01$), demonstrating that Fibulin-4 deletion results in the observed defects in mitochondrial respiration similar to those in the Fibulin-4$^{R/R}$ VSMCs. We did not observe significant changes in the ECAR compared to Fibulin-4$^{+/+}$ VSMCs (data not shown).

We were interested whether the same decreased OCR was present in VSMCs from other aneurysmal syndromes. This prompted us to first measure mitochondrial respiration in VSMCs obtained from the Tgfbr-1$^{M318R/+}$ mouse, a model for Loeys-Dietz syndrome (LDS).[28] Similar to Fibulin-4$^{R/R}$ and Fibulin-4^{SMKO} VSMCs, Tgfbr-1$^{M318R/+}$ VSMCs showed a reduced basal and maximal OCR compared to Tgfbr-1$^{+/+}$ VSMCs (*Figure 2F*). We did not observe an obvious decrease in ECAR as seen for Fibulin-4$^{R/R}$ VSMCs (data not shown). To examine whether oxygen consumption is also affected in cells of Marfan and Loeys-Dietz patients, we set out to measure mitochondrial respiration in patient cell lines. Although we did not have access to human VSMCs, we were able to obtain human fibroblasts from aneurysmal patients with Fibrillin-1 (FBN1 c.4817-1G>A: FBN1 ex 39), TGFβ receptor 2 (TGFBR2 c.1573delA: TGFBR2 ex 07), and Smad3 (SMAD3 c.859C>T, p.R287W: SMAD3 ex 9) mutations, as well as three control cell lines. We next used the human patient fibroblasts to perform seahorse experiments. Interestingly, all three patient cell lines showed a significantly reduced basal and maximum OCR compared to the control cell lines (*Figure 2G,H*). From these data, we conclude that the altered mitochondrial oxygen consumption

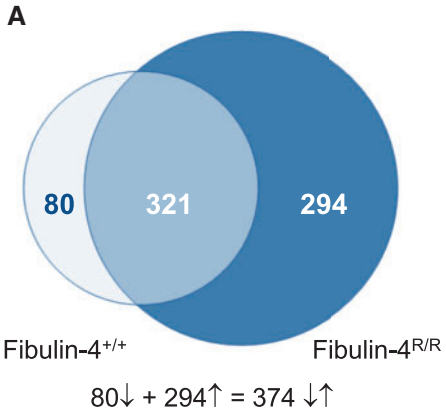

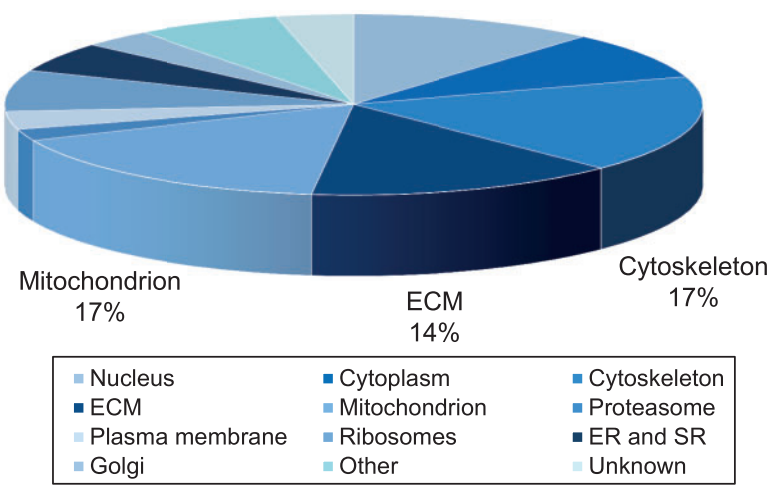

C

Upstream Regulator	Description	Molecule Type	Pred. Act. State	Bias-corr z-score	p-value overlap
TGFB1	Transforming growth factor, beta 1	growth factor	Activated	3,54	2,10E-15
TP53	Tumor protein p53	transcription regulator	Activated	2,31	1,53E-04
AGT	Angiotensinogen	growth factor	Activated	2,10	2,69E-06
SREBF2	Sterol regulatory element binding transcription factor 2	transcription regulator	Inhibited	-3,76	1,79E-04
MLXIPL	MLX interacting protein-like	other	Inhibited	-3,27	3,03E-06
SREBF1	Sterol regulatory element binding transcription factor 1	transcription regulator	Inhibited	-3,22	5,45E-09
HNF4A	Hepatocyte nuclear factor 4, alpha	transcription regulator	Inhibited	-3,00	8,66E-07
T3-TR-RXR	TR/RXR Activation complex	complex	Inhibited	-2,93	4,98E-03
PDGF BB	PDGF complex	complex	Inhibited	-2,19	2,42E-04
ATP7B	ATPase, Cu++ transporting, beta polypeptide	transporter	Inhibited	-2,16	4,15E-03
IRF4	Interferon regulatory factor 4	transcription regulator	Inhibited	-2,05	1,74E-03
PPARA	Peroxisome proliferator-activated receptor alpha	ligand-dependent nuclear receptor	Inhibited	-2,00	1,00E-09

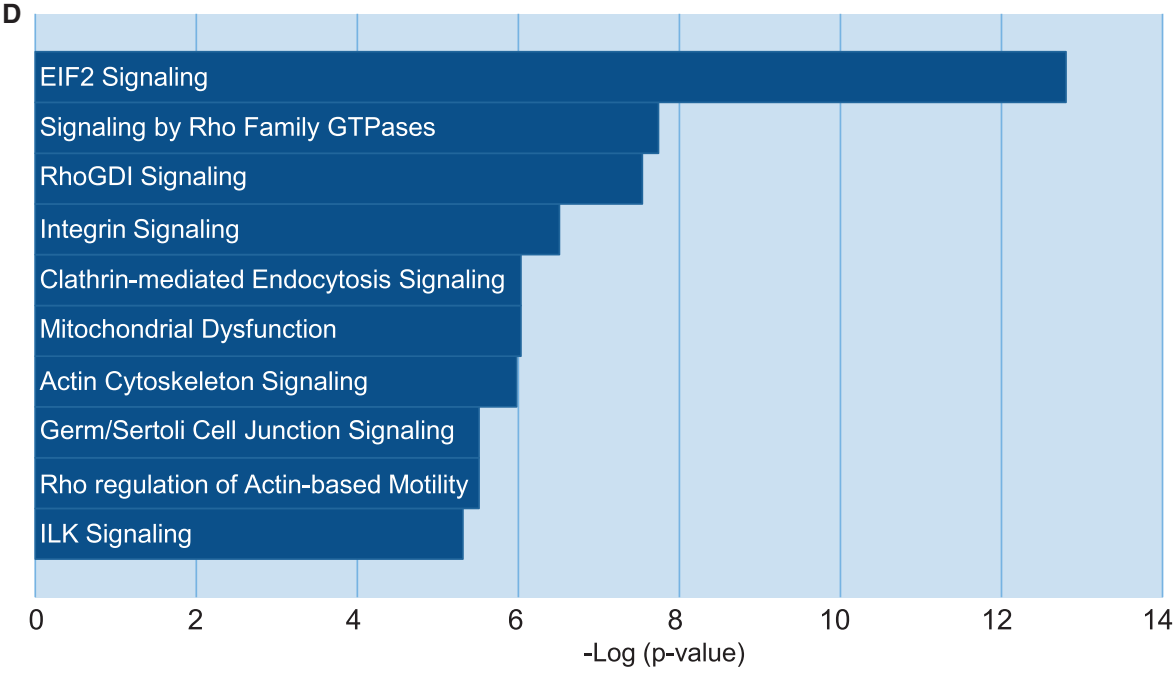

Figure 1 Proteomics analysis of Fibulin-$4^{R/R}$ and Fibulin-$4^{+/+}$ thoracic aortas identifies mitochondrial function as potentially affected. (*A*) Venn diagram comparison of proteins identified in Fibulin-$4^{+/+}$ (left circle) and Fibulin-$4^{R/R}$ (right circle) aortas; on the left side proteins over-represented in Fibulin-$4^{+/+}$ aortas (light blue), on the right side proteins over-represented in Fibulin-$4^{R/R}$ aortas (dark blue). Overlap between the two circles represents proteins that exhibit no chance between the two groups. (*B*) Pie graph of GO-term distribution of proteins differentially regulated in Fibulin-$4^{R/R}$ compared to Fibulin-$4^{+/+}$ aorta. Cytoskeleton (17%), extracellular matrix (ECM, 14%), and mitochondria (17%) together comprise 48% of differentially regulated

in aneurysms is not restricted to Fibulin-4 mutations per se but is present in VSMCs and fibroblasts of multiple thoracic aneurysmal aorta syndromes.

3.3 Complexes I, III, IV, and V levels and activity in Fibulin-4$^{R/R}$ VSMCs and tissues

To investigate whether mitochondrial localization was affected by Fibulin-4 mutation, we first stained two independent Fibulin-4$^{R/R}$ and Fibulin-4$^{+/+}$ VSMC cell lines used in the Seahorse experiments with Mitotracker CMX Ros and SiR-Actin. We observed no differences in mitochondrial localization or obvious differences in cytoskeletal composition between Fibulin-4 mutant or control cell lines (*Figure 3A*). We next performed fluorescence-activated cell sorting (FACS) experiments using Fibulin-4$^{R/R}$ and Fibulin-4$^{+/+}$ VSMCs with the Mitotracker CMX Ros probe to determine the number of mitochondria per cell. From this analysis we observed no differences in mitochondrial signals, indicating no change in number of mitochondria per cell (*Figure 3B*). The observed differences in mitochondrial function in Fibulin-4$^{R/R}$ and Fibulin-4$^{+/+}$ cells prompted us to examine mitochondrial structure in VSMCs of the aorta by electron microscopy (EM). The mitochondrial ultrastructure in Fibulin-4$^{+/+}$ and Fibulin-4$^{R/R}$ cells appeared similar, although the Fibulin-4$^{R/R}$ mitochondria seemed somewhat reduced in size (*Figure 3C*).

The clear differences in mitochondrial respiration, without affecting the number of mitochondria per cell, could imply an altered mitochondrial mass (i.e. total mitochondrial volume in the cell) in Fibulin-4$^{R/R}$ VSMCs. In turn, this could indicate less mitochondrial complexes per cell, leading to decreases in OCR. However, the proteomics data showed a higher expression of mitochondrial complex proteins involved in OXPHOS. To investigate expression of mitochondrial complex proteins, we performed western blot analysis using thoracic aorta tissue with an antibody cocktail directed against five specific OXPHOS I-V complex subunits that are labile when its complex is not assembled. Interestingly, when compared to Fibulin-4$^{+/+}$, the protein level of Complexes I through IV was significantly ($P < 0.05$) increased in Fibulin-4$^{R/R}$ aortas, whereas Complex V showed no significant change (*Figure 3D,E*). This is in agreement with the results from the proteomics analysis which showed that several individual mitochondrial complex proteins are upregulated. This could indicate a partial compensatory reaction of the respiratory electron transport chain (ETC) to counteract the decrease in mitochondrial mass. We also performed this western blot on Fibulin-4^{SMKO} aortic extracts and littermate controls, to see if deleting Fibulin-4 in VSMCs alone could result in overexpression of these complexes. Indeed, we observed overexpression of Complexes I–IV in Fibulin-4^{SMKO} (Supplementary material online, *Figure S1D*), however this was not a significant difference, indicating that other cells in the aorta of Fibulin-4$^{R/R}$ animals may also contribute to this effect.

To see if decreased OCR is not limited to the aorta, we measured respiratory capacity in aorta, heart, muscle, and liver of Fibulin-4$^{+/+}$ and Fibulin-4$^{R/R}$ animals. Unfortunately, we were unable to determine OCR in aortic extracts, probably due to rigidity of the tissue because of ECM content. Nevertheless, heart and skeletal muscle, containing large amounts of muscle cells and highly dependent on mitochondrial activity, both showed a significantly lower OCR (*Figure 3F*). The liver did not show a lower, but somewhat higher (non-significant) OCR (*Figure 3F*), which we would expect if the observed OCR decrease is muscle cell specific. To determine whether the decreased oxygen consumption was due to reduced mitochondrial complex activity, we measured individual Complexes I, III, IV, and V activities (II is not subject to change), but observed no significant change (*Figure 3G*). These data fit with the observation that more Complexes I–IV proteins are present in the aorta (*Figure 3D,E*). Taken together, we can conclude that the reduced oxygen consumption is not due to lower complex activity.

3.4 Molecular imaging reveals increased ROS in the aorta of Fibulin-4$^{R/R}$ animals

The observed imbalance between mitochondrial mass and the expression and activity of mitochondrial enzyme complexes may lead to an increase in generation of reactive oxygen species (ROS). In this context, we did observe a somewhat lower ADP ratio in Fibulin-4$^{R/R}$ muscular tissues (data not shown), which would imply less efficient ATP production that could lead to more radical formation. To investigate if indeed more radicals are present, we performed molecular imaging using the L-012 probe. This probe emits a luminescent signal upon interaction with reactive oxygen and nitrogen species that is quantified using an IVIS spectrum imaging system. We injected Fibulin-4$^{R/R}$ and Fibulin-4$^{+/+}$ animals with the L-012 probe and recorded the luminescent signal from the opened chest of mice after 1 h to determine the signal localization. Experiments were performed three times with each Fibulin-4$^{R/R}$ animal matched to a Fibulin-4$^{+/+}$ littermate control. We observed a significant increase in average L-012-derived luminescence in Fibulin-4$^{R/R}$ aortas compared to Fibulin-4$^{+/+}$ (*Figure 4A,B*, $P < 0.05$). Consistently, staining of Fibulin-4$^{R/R}$ aortic sections with the superoxide indicator DHE showed increased 2-OH-ethidium fluorescence compared to Fibulin-4$^{+/+}$, indicative of increased superoxide levels (*Figure 4C*, $P < 0.05$). Together, these data show that ROS levels are elevated in Fibulin-4$^{R/R}$ aortas.

3.5 Systemic metabolic analyses indicate a metabolic switch towards fatty acid oxidation in Fibulin-4$^{R/R}$ animals

Previous gene expression studies performed on young Fibulin-4$^{R/R}$ animals gave insight into the mechanism of aneurysm formation, amongst which were cytoskeleton re-organization and perturbed TGFβ signalling.[13] As we observed many changes at the protein level pointing towards mitochondrial involvement, we wondered whether this would also be reflected at the transcriptional level. Additionally we were interested whether gene expression profiles could point to potential mechanisms and targets involved. Therefore, we performed gene expression analyses on 3-month old Fibulin-4$^{+/+}$ and Fibulin-4$^{R/R}$ thoracic aortas by using GeneChip mouse exon 1.0 ST arrays (Affymetrix). The obtained gene expression differences (*P*-value of 0.03; fold change 1.2) were

Figure 1 Continued

proteins. (*C*) Table depicting predicted activation or inhibition of Upstream Regulators (-2> bias-corrected z-score > 2, *P*-value <0.01), derived from an IPA analysis based on differentially regulated proteins in Fibulin-4$^{R/R}$ compared to Fibulin-4$^{+/+}$ aortas. Notably, TGFβ1 and Angiotensinogen (AGT) are predicted to be upregulated, which is known from literature, thus validating this prediction approach. (*D*) Graph depicting the top 10 significantly changed ($P < 0.01$) canonical pathways, derived from an IPA analysis based on the differentially regulated proteins in Fibulin-4$^{R/R}$ compared to Fibulin-4$^{+/+}$ aortas. Mitochondrial dysfunction is the 6th most significantly changed canonical pathway.

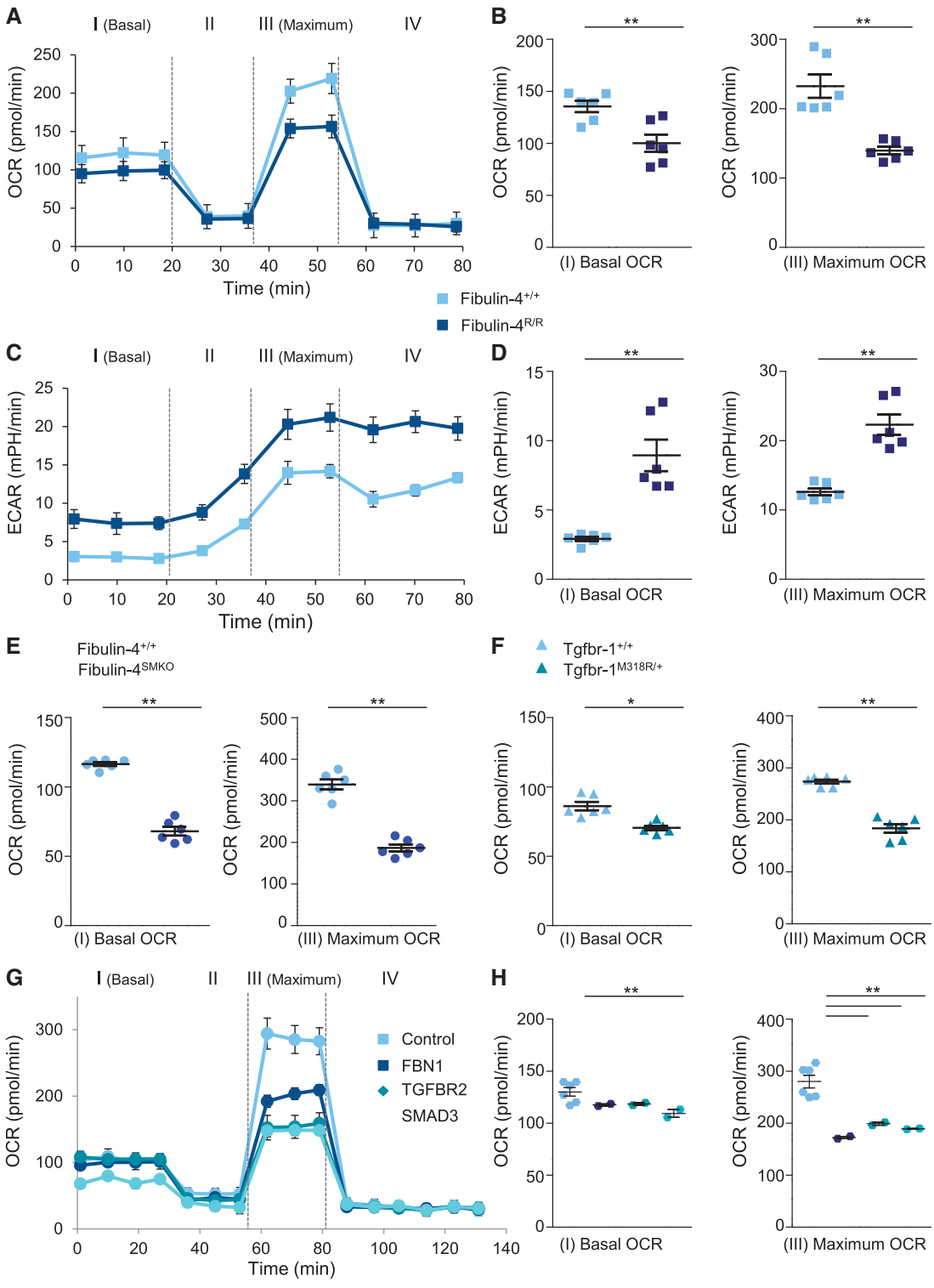

Figure 2 Reduced OCR and increased ECAR in Fibulin-4 deficient VSMCs. (*A*) Graph depicting the oxygen consumption rate (OCR) in Fibulin-$4^{R/R}$ VSMCs (dark blue squares) and Fibulin-$4^{+/+}$ VSMCs (light blue squares) at basal level (I) and after addition of oligomycin, a Complex V inhibitor (II), FCCP, an OXPHOS uncoupler, for maximum OCR measurement (III), and a combination of rotenone (Complex I inhibitor) and antimycin A (Complex III inhibitor), showing potential OCR differences not due to mitochondria (IV). (*B*) Both at basal level (I) and at maximum oxygen consumption level (III) Fibulin-$4^{R/R}$ VSMCs show a significantly lower OCR compared to Fibulin-$4^{+/+}$ ($P < 0.01$, Student's *t*-test), indicating altered mitochondrial function. The scatter plot shows absolute OCR levels from three experiments that were performed in two independent cell lines per genotype. (*C*) Graph depicting the extracellular acidification rate (ECAR) in Fibulin-$4^{R/R}$ and Fibulin-$4^{+/+}$ VSMCs. (*D*) ECAR is significantly elevated in Fibulin-$4^{R/R}$ compared to Fibulin-$4^{+/+}$ VSMCs ($P < 0.01$, Student's *t*-test), quantified at basal (I) and maximum OCR (III). The scatter plot shows ECAR levels from three experiments that were performed in two independent cell lines per genotype. (*E*) Scatter plots showing basal (I) and maximum (III) OCR levels in Fibulin-4^{SMKO} VSMCs (dark blue circles), which are knock-out for Fibulin-4 in VSMCs specifically, and Fibulin-$4^{+/+}$ VSMCs (light blue circles), for three experiments that were performed in two

uploaded and analysed in IPA. Canonical pathway analysis pointed towards numerous pathway changes related to metabolism (see *Figure 5A* for the top 10); out of the 30 canonical pathways predicted to be significantly changed ($P < 0.01$), 73% are directly involved in metabolic processes (data not shown). Moreover, when we examine the first 10 networks significantly changed based on our gene dataset, at the first position we find 'Energy Production/Lipid Metabolism/Small Molecule Biochemistry' (Supplementary material online, *Figure S3*).

To investigate if metabolic changes observed in the thoracic aorta are also reflected systemically in the mouse, we first analysed body weights of the mice. Indeed, Fibulin-$4^{R/R}$ animals ($n = 38$) had a significantly lower body weight than Fibulin-$4^{+/+}$ animals (*Figure 5B*, $P < 0.05$). Next, we examined three important metabolic parameters: glucose, lactate, and ketones in blood of non-fasted Fibulin-$4^{+/+}$ and Fibulin-$4^{R/R}$ animals. These parameters together shed light on the main metabolic processes used to generate ATP. Both blood glucose levels as well as blood lactate did not show significant differences between the two genotypes (*Figure 5C,D*). However, blood ketone levels were significantly lower in Fibulin-$4^{R/R}$ compared to Fibulin-$4^{+/+}$ animals (*Figure 5E*, $P < 0.01$). Interestingly, in our gene expression analysis, we found that the key enzyme responsible for breakdown of ketones, is significantly upregulated in the aorta (3-oxoacid CoA transferase, OXCT1, 1.3-fold, $P = 0.03$, Supplementary material online, *Figure S6A*). In addition, IPA analysis revealed many genes involved in the citric acid cycle [tricarboxylic acid cycle (TCA)] pathway significantly downregulated in Fibulin-$4^{R/R}$ compared to Fibulin-$4^{+/+}$ aortas (Supplementary material online, *Figure S4A*).

The liver is a central organ involved in metabolism and adjusts metabolic processes to energy demands of the different tissues within an organism. Since ketones are products of fatty acid oxidation in the liver, we next performed oil-red-o staining on livers isolated from Fibulin-$4^{+/+}$ and Fibulin-$4^{R/R}$ animals ($n = 5$ per group) that were normally fed. These animals did not show signs of malnutrition, or malabsorption of food in the intestine, and the liver showed no overt abnormalities on H&E-stained sections (data not shown). Yet, livers of Fibulin-$4^{R/R}$ animals clearly showed reduced oil-red-o staining in all five animals examined as compared to their respective Fibulin-$4^{+/+}$ littermates (*Figure 5F*, $P < 0.01$). In contrast, periodic acid-Schiff (PAS) staining for glycogen showed the exact opposite; all five Fibulin-$4^{R/R}$ animals showed increased glycogen accumulation compared to their respective Fibulin-$4^{+/+}$ littermates (*Figure 5G*, $P < 0.01$). We found no direct evidence for malfunctioning mitochondria of the liver regarding the process of OXPHOS, since these livers showed normal OCR, and immunoblots of liver lysates from Fibulin-$4^{R/R}$ and Fibulin-$4^{+/+}$ animals did not show differences in the amount of the various OXPHOS complexes (Supplementary material online, *Figure S4B*). This could be due to absence or low expression of Fibulin-4 in the liver. Thus, based on the reduction of fatty acids in the liver together with reduction of ketones in the blood, it is likely that metabolism in the liver of Fibulin-$4^{R/R}$ mice has shifted to fatty acid β-oxidation and the production of ketone bodies, to meet the altered demand in energy carrier type (ketone bodies vs. glucose) by the aneurysmal aorta.

We next compared the gene expression data of newborn Fibulin-$4^{R/R}$ aortas, previously published by Hanada *et al.*,[13] with the gene expression data of adult Fibulin-$4^{R/R}$ aortas. This comparison resulted in 106 overlapping, significantly regulated genes (FC > 1.2; $P < 0.05$) used for IPA analysis, of which 99 were regulated in the same direction. Canonical pathway analysis showed processes involved in fat and glucose metabolism significantly regulated, such as atherosclerosis signalling, PPARα/RXRα signalling and glycolysis, in common between newborn and adult aortas (Supplementary material online, *Figure S5A*), which may hint to processes that are important from an early time point on for aneurysm formation in these animals. Moreover, upstream regulator analysis predicted, amongst others, TGFB1, miR-29b, and PPARG to be significantly differentially regulated (Supplementary material online, *Figure S5B*). Interestingly, TGFB1 and miR-29b have previously been published to be altered in Fibulin-$4^{R/R}$ aortas,[13,31,32] and are here also found to be important key regulators. PPARG was not previously identified but plays an important role in fat metabolism. As we observed changes in fat and glycogen deposition in adult Fibulin-$4^{R/R}$ livers compared to Fibulin-$4^{+/+}$ livers, we performed the same staining on newborn livers. However, we did not observe obvious changes in fat or glycogen deposition between Fibulin-$4^{R/R}$ and Fibulin-$4^{+/+}$ newborn livers (Supplementary material online, *Figure S5C*, $n = 5$ per genotype). These data together could indicate that the aneurysmal induced changes in metabolic processes may precede the metabolic changes in the liver.

3.6 Reduced PGC1α expression and activity in aortas and VSMCs of Fibulin-$4^{R/R}$ animals

Since we discovered changes in mitochondrial function in thoracic aortas of Fibulin-$4^{R/R}$ animals, it would be interesting to know which process or subset of factors is responsible. To investigate this, we looked at upstream regulators that are predicted to be significantly changed based on the gene expression data in the thoracic aorta of Fibulin-$4^{R/R}$ animals. Interestingly, PGC1α and PGC1β (peroxisome proliferator-activated receptor gamma, coactivator 1 α and β) as well as PPARα, PPARδ and PPARγ (peroxisome proliferator-activated receptor α, δ, and γ) were predicted to be significantly downregulated (*Table 2*). In addition, we noticed that they were also all significantly downregulated at the gene expression level, except for PPARδ, which showed no significant change (*Table 2*). Next, we performed real-time PCR analysis to check the mRNA expression levels of PGC1α, PGC1β, PPARα, and PPARγ in thoracic aorta extracts of Fibulin-$4^{R/R}$ and Fibulin-$4^{+/+}$ animals. We found

Figure 2 Continued

independent cell lines per genotype. Fibulin-4^{SMKO} VSMCs show a significantly lower OCR compared to Fibulin-$4^{+/+}$ ($P < 0.01$, Student's *t*-test). (*F*) Scatter plots showing basal (I) and maximum (III) OCR levels in Tgfbr-$1^{M318R/+}$ (dark blue triangles) and Tgfbr-$1^{+/+}$ VSMCs (light blue triangles), of three experiments that were performed in two independent cell lines per genotype. Both at basal (I) and at maximum OCR level (III) Tgfbr-$1^{M318R/+}$ VSMCs show a significantly lower OCR compared to Tgfbr-$1^{+/+}$ ($P < 0.01$, Student's *t*-test). (*G*) Graph depicting the oxygen consumption rate (OCR) in three different human fibroblast cell lines derived from aneurysmal patients with a Fibrillin-1 (FBN1, dark blue squares), TGFβ receptor 2 (TGFBR2, blue diamonds), and SMAD3 (light blue circles) mutation, as well as the mean of three control cell lines (light blue squares). (*H*) Scatter plots showing basal (I) and maximum (III) OCR levels, which are significantly lower for the human mutant fibroblasts compared to control ($P < 0.01$, Student's *t*-test). OCR observations were made in two independent experiments, in case of the controls for three independent cell lines. All results are expressed as mean ± SEM.

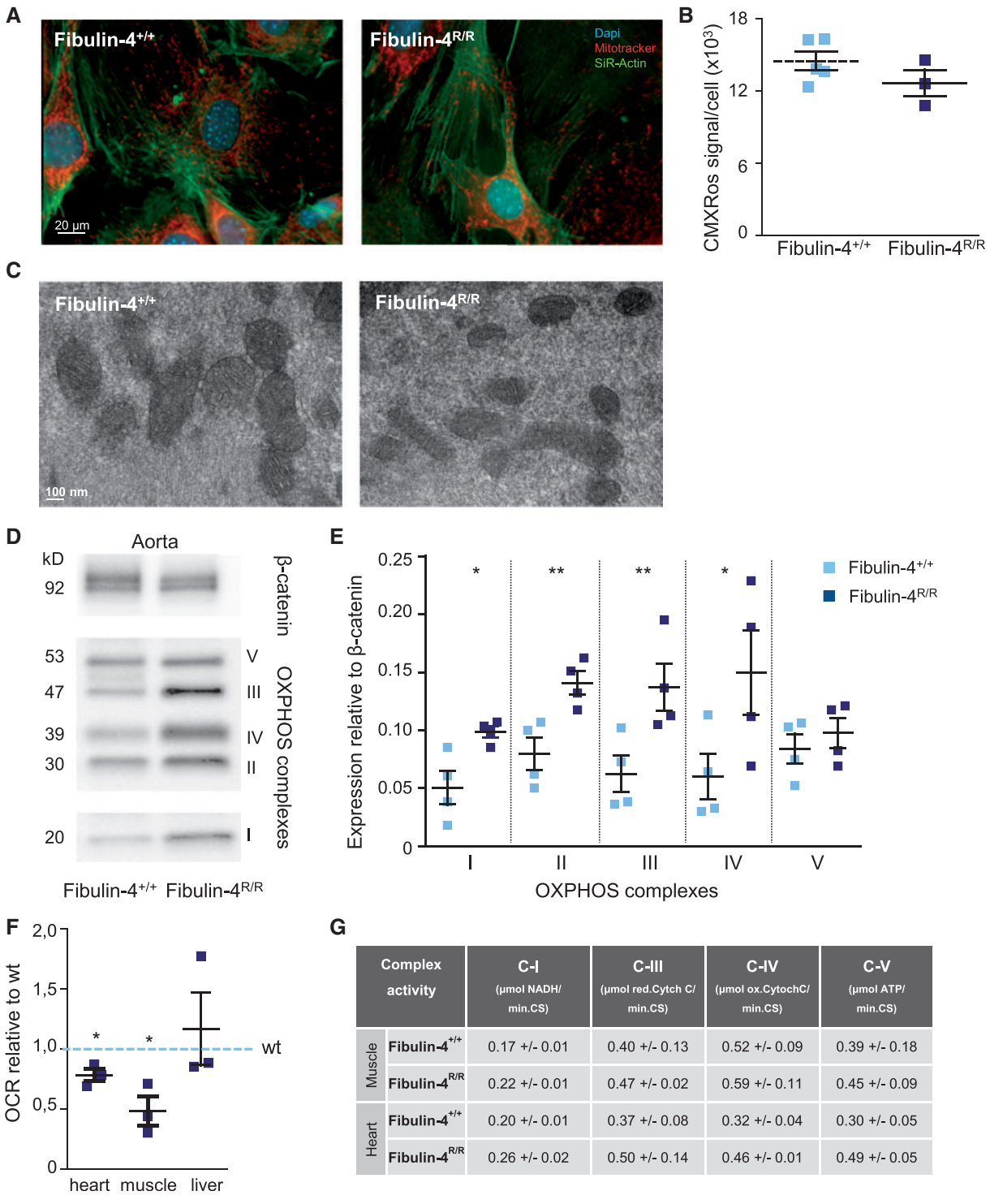

	Complex activity	C-I (µmol NADH/ min.CS)	C-III (µmol red.Cytch C/ min.CS)	C-IV (µmol ox.CytochC/ min.CS)	C-V (µmol ATP/ min.CS)
Muscle	Fibulin-4$^{+/+}$	0.17 +/- 0.01	0.40 +/- 0.13	0.52 +/- 0.09	0.39 +/- 0.18
	Fibulin-4$^{R/R}$	0.22 +/- 0.01	0.47 +/- 0.02	0.59 +/- 0.11	0.45 +/- 0.09
Heart	Fibulin-4$^{+/+}$	0.20 +/- 0.01	0.37 +/- 0.08	0.32 +/- 0.04	0.30 +/- 0.05
	Fibulin-4$^{R/R}$	0.26 +/- 0.02	0.50 +/- 0.14	0.46 +/- 0.01	0.49 +/- 0.05

Figure 3 Mitochondrial size and complexes are affected in the thoracic aorta of Fibulin-4$^{R/R}$ animals. (*A*) Mitotracker and SiR-Actin staining of Fibulin-4$^{R/R}$ and Fibulin-4$^{+/+}$ VSMCs showing a very similar distribution and pattern. The white line indicates a length of 20 µm. (*B*) Scatter plot depicting mitotracker (CMXRos) signal per cell, a measure for mitochondrial number per cell. No significant difference was observed (Student's *t*-test). Mitotracker experiments were performed for $n = 3$ (Fibulin-4$^{R/R}$) and n = 5 (Fibulin-4$^{+/+}$) cell lines, with the same result. (*C*) Representative electron micrographs of VSMCs in Fibulin-4$^{+/+}$ and Fibulin-4$^{R/R}$ aortas, showing no obvious structural changes, except for smaller mitochondrial size in the latter. The white line indicates a length of 100 nm. (*D*) Representative western blot for mitochondrial Complexes I–V proteins in Fibulin-4$^{+/+}$ and Fibulin-4$^{R/R}$ aorta lysates with β-catenin as loading control. Please note that Complex IV is lower in size than Complex III. Although detection was done on the same western blot, it is divided into three pieces as the pictures were taken with different exposure times; 1, 2, and 5 min for β-catenin, Complexes II–V and Complex I, respectively. (*E*) Quantification of the different complexes for wild-type and Fibulin-4$^{R/R}$ aortas, showing significant increases in Complexes I–IV in Fibulin-4$^{R/R}$ aortas compared to wild-type ($n = 4$ per genotype, $^{*}P < 0.05$; $^{**}P < 0.01$, Student's *t*-test on log-transformed data). (*F*) OCR measurements in heart, muscle, and liver, showing lower OCR in Fibulin-4$^{R/R}$ animals compared to their respective Fibulin-4$^{+/+}$ littermates ($n = 3$ per genotype, $P < 0.05$, Student's *t*-test on log-transformed data). (*G*) Complex activity measurements in Fibulin-4$^{+/+}$ and Fibulin-4$^{R/R}$ heart and muscle showing no significant difference ($n = 3$ per genotype). All results are expressed as mean ± SEM.

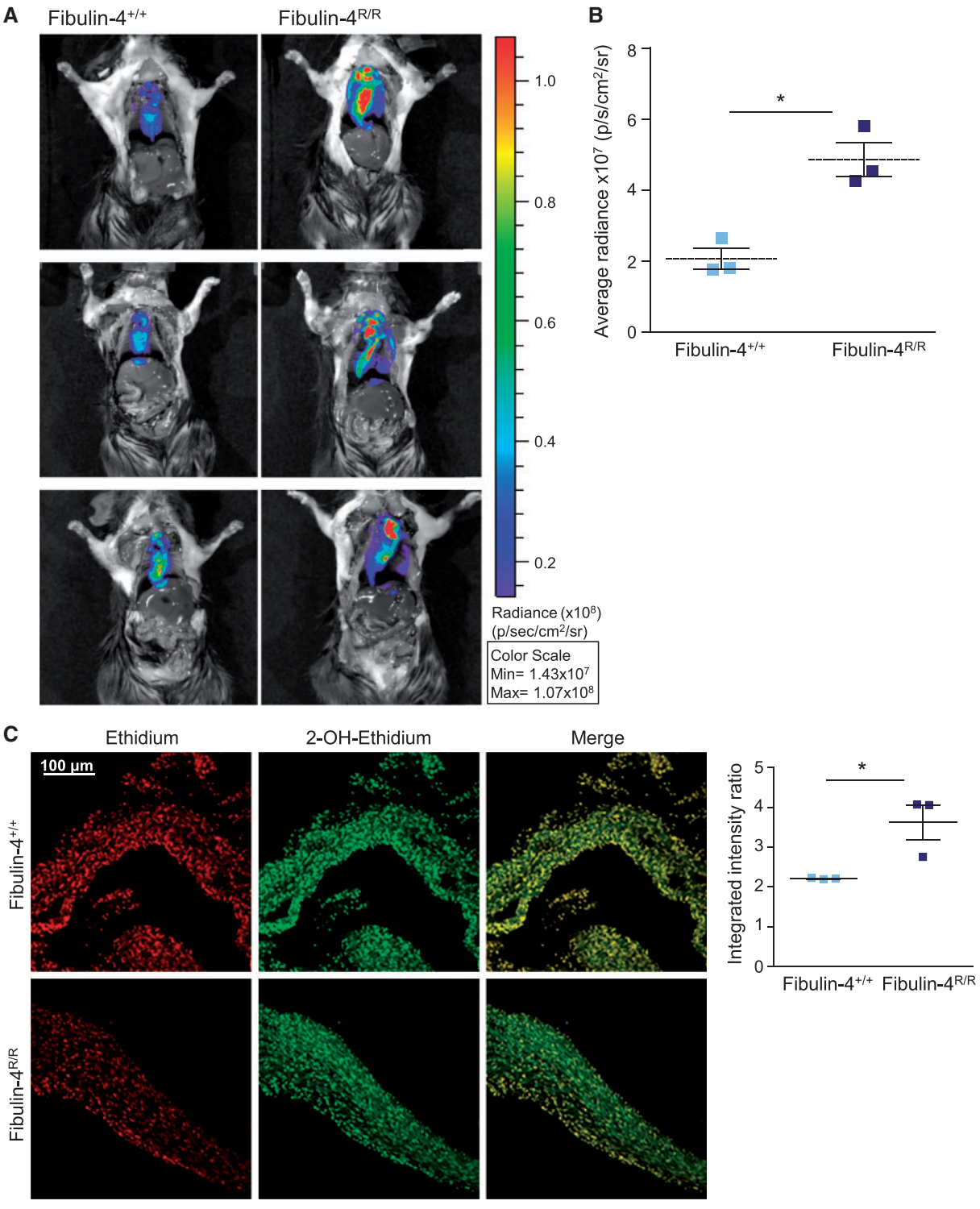

Figure 4 Molecular imaging reveals increased ROS levels in Fibulin-$4^{R/R}$ animals. (*A*) Representative pictures of three independent experiments showing increased LO12 probe signal intensity (emits light after ROS binding) in Fibulin-$4^{R/R}$ (right) animals compared to respective Fibulin-$4^{+/+}$ (left) littermates. (*B*) Quantification of the average radiance at the site of the aorta, a measure for the amount of ROS reacting with LO12 probe, shows significantly higher levels in the Fibulin-$4^{R/R}$ compared to Fibulin-$4^{+/+}$ mice ($n = 3$ per genotype, $^*P = 0.01$, Student's *t*-test). (*C*) Left panel: representative sections of DHE staining for superoxide anion, in aortic sections from Fibulin-$4^{R/R}$, counterstained with ethidium for DNA content (red), show increased 2-OH-DHE fluorescence (green) compared to Fibulin-$4^{+/+}$ as shown in the merged picture (left, predominantly green in Fibulin-$4^{R/R}$ vs. yellow in Fibulin-$4^{+/+}$). The white line indicates a length of 100 µm. Right panel: scatter plot depicting the integrated intensity ratio for Fibulin-$4^{+/+}$ and Fibulin-$4^{R/R}$, showing an increase in the latter ($n = 3$ per genotype, $^*P < 0.05$, Student's *t*-test). All results are expressed as mean ± SEM.

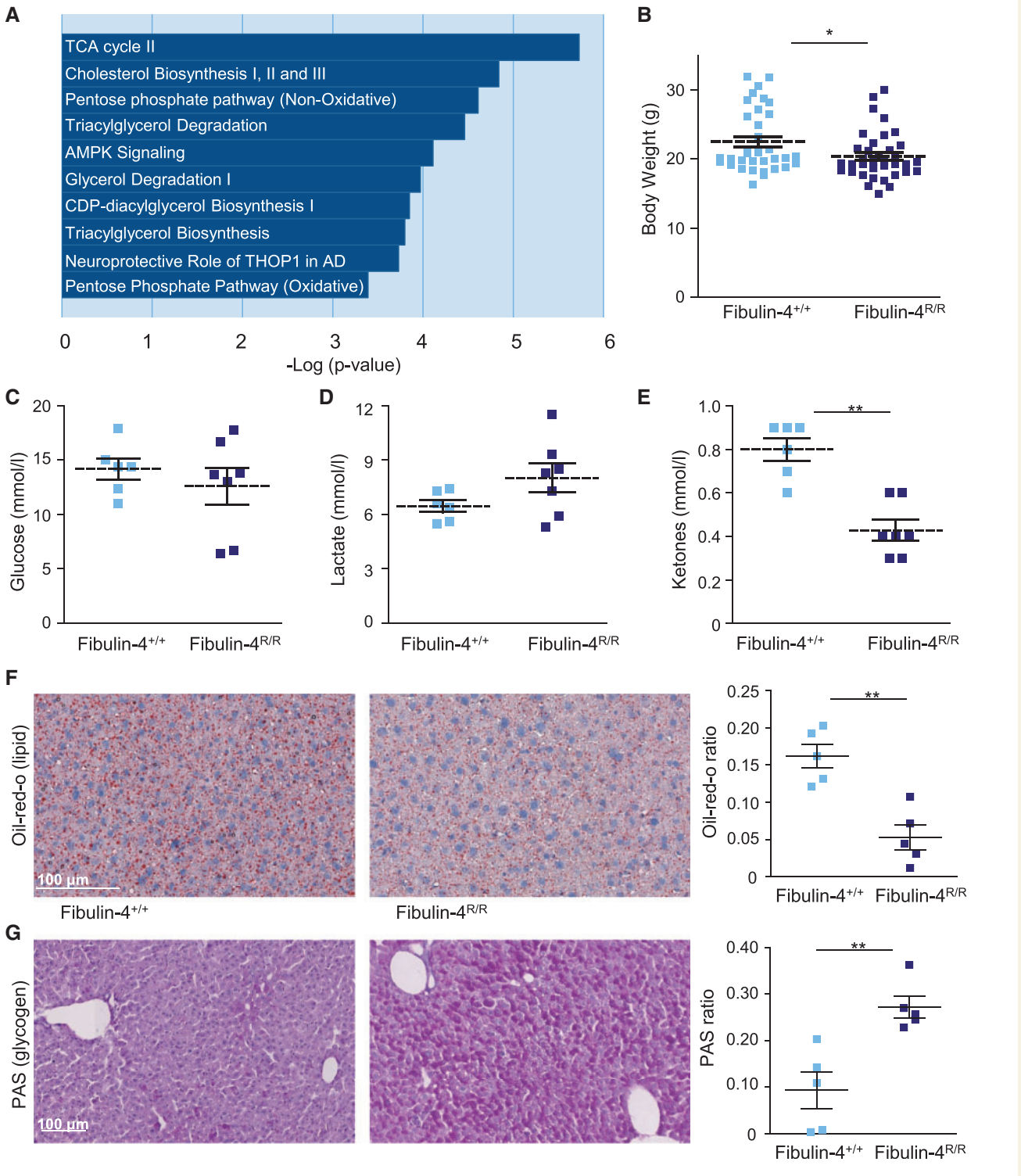

Figure 5 Gene expression analysis and metabolic parameters show altered metabolism in Fibulin-4$^{R/R}$ animals. (*A*) Graph depicting the top 10 significantly changed ($P < 0.01$) canonical pathways, derived from an IPA analysis based on the differentially regulated genes between Fibulin-4$^{R/R}$ and Fibulin-4$^{+/+}$ aortas, showing an over-representation of pathways involved in energy metabolism. (*B*) Scatter plot depicting body weights of Fibulin-4$^{R/R}$ and Fibulin-4$^{+/+}$ animals, showing significant reduction in Fibulin-4$^{R/R}$ compared to Fibulin-4$^{+/+}$ animals at 3 months ($n = 38$ and 35, respectively, $P < 0.05$, Student's *t*-test). (*C–E*) Scatter plots depicting glucose (Fibulin-4$^{+/+}$ $n = 6$, Fibulin-4$^{R/R}$ $n = 7$), lactate (Fibulin-4$^{+/+}$ $n = 6$, Fibulin-4$^{R/R}$ $n = 5$) and ketone levels (Fibulin-4$^{+/+}$ $n = 6$, Fibulin-4$^{R/R}$ $n = 7$), respectively, in blood of Fibulin-4$^{R/R}$ and Fibulin-4$^{+/+}$ animals, showing a significant reduction in serum ketone levels for Fibulin-4$^{R/R}$ animals ($P < 0.01$, Student's *t*-test). (*F*) Representative pictures of oil-red-o staining for lipids in Fibulin-4$^{R/R}$ and Fibulin-4$^{+/+}$ livers (left), and quantification of oil-red-o ratio (right). Compared to their Fibulin-4$^{+/+}$ littermates, Fibulin-4$^{R/R}$ show decreased oil-red-o staining in the liver ($P < 0.01$, Student's *t*-test) ($n = 5$ per genotype). (*G*) Representative pictures of PAS staining for glycogen in Fibulin-4$^{R/R}$ and Fibulin-4$^{+/+}$ livers (left) and quantification of PAS ratio (right). Compared to their Fibulin-4$^{+/+}$ littermates, Fibulin-4$^{R/R}$ show increased PAS staining in their livers ($P < 0.01$) ($n = 5$ per genotype). The white line indicates a length of 100 µm. All results are expressed as mean ± SEM.

Table 2 Upstream regulator analysis based on IPA gene expression analysis of Fibulin-4$^{R/R}$ vs. Fibulin-4$^{+/+}$ aortas.

Upstream regulator	Description	Molecule type	Pred. Act. State	Bias-corrected z-score	*P*-value overlap	FC in dataset
PPARG	Peroxisome proliferator-activated receptor gamma	Ligand-dependent nuclear receptor	Inhibited	-3.918	4.28E-17	-1.946
SREBF2	Sterol regulatory element binding transcription factor 2	Transcription regulator	Inhibited	-3.28	1.74E-11	
SCAP	SREBF chaperone	Other	Inhibited	-3.212	6.40E-15	
ATP7B	ATPase, Cu++ transporting, beta polypeptide	Transporter	Inhibited	-3.194	6.94E-07	-1.276
PPARGC1A	Peroxisome proliferator-activated receptor gamma, coactivator 1 alpha	Transcription regulator	Inhibited	-3.062	8.97E-10	-2.409
SREBF1	Sterol regulatory element binding transcription factor 1	Transcription regulator	Inhibited	-3.046	3.10E-15	-1.288
PPARA	Peroxisome proliferator-activated receptor alpha	Ligand-dependent nuclear receptor	Inhibited	-2.968	2.60E-16	-1.720
CTNNA (group)	Alpha catenin	Group	Inhibited	-2.946	9.42E-03	
NR1H3	Nuclear receptor subfamily 1, group H, member 3	Ligand-dependent nuclear receptor	Inhibited	-2.904	1.90E-04	-1.522
COL18A1	Collagen, type XVIII, alpha 1	Other	Inhibited	-2.68	1.79E-01	
INSR	Insulin receptor	Kinase	Inhibited	-2.509	2.65E-06	-1.268
NR3C1	Nuclear receptor subfamily 3, group C, member 1 (glucocorticoid receptor)	Ligand-dependent nuclear receptor	Inhibited	-2.455	7.40E-03	
NR1H2	Nuclear receptor subfamily 1, group H, member 2	Ligand-dependent nuclear receptor	Inhibited	-2.341	9.07E-07	
NT5E	5'-Nucleotidase, ecto (CD73)	Phosphatase	Inhibited	-2.328	2.04E-03	1.400
PPARD	Peroxisome proliferator-activated receptor delta	Ligand-dependent nuclear receptor	Inhibited	-2.196	1.16E-04	
KLF15	Krüppel-like factor 15	Transcription regulator	Inhibited	-2.098	5.31E-04	
BMP7	Bone morphogenetic protein 7	Growth factor	Inhibited	-2.094	8.14E-03	
HNF4A	Hepatocyte nuclear factor 4, alpha	Transcription regulator	Inhibited	-2.072	1.10E-02	
PPARGC1B	Peroxisome proliferator-activated receptor gamma, coactivator 1 beta	Transcription regulator	Inhibited	-2.038	1.19E-06	-1.569
INSIG2	Insulin induced gene 2	Other	Activated	2.129	1.10E-09	1.276
FGF19	Fibroblast growth factor 19	Growth factor	Activated	2.13	6.29E-05	
NRIP1	Nuclear receptor interacting protein 1	Transcription regulator	Activated	2.185	4.81E-12	
HOXC6	Homeobox C6	Transcription regulator	Activated	2.219	4.30E-02	-1.411
KRT17	Keratin 17	Other	Activated	2.468	8.52E-03	
PTGS2	Prostaglandin-endoperoxide synthase 2	Enzyme	Activated	2.505	2.35E-01	1.618
LTα1β2	Lymphotoxin-alpha1-beta2	Complex	Activated	2.546	1.01E-03	
SPI1	Spleen focus forming virus (SFFV) proviral integration oncogene spi1	Transcription regulator	Activated	2.632	1.44E-02	1.621
PI3K (complex)	Phosphatidylinositol 3-kinase	Complex	Activated	2.65	9.19E-02	
WNT1	Wingless-type MMTV integration site family, member 1	Cytokine	Activated	2.708	3.01E-03	
OSM	Oncostatin M	Cytokine	Activated	2.708	1.99E-04	
POR	P450 (cytochrome) oxidoreductase	Enzyme	Activated	2.723	5.04E-07	-1.626
SPP1	Secreted phosphoprotein 1	Cytokine	Activated	2.748	7.42E-06	4.884
RET	Ret proto-oncogene	Kinase	Activated	2.772	6.63E-04	

Continued

Table 2 *Continued*

Upstream regulator	Description	Molecule type	Pred. Act. State	Bias-corrected z-score	*P*-value overlap	FC in dataset
CSF2	Colony stimulating factor 2 (granulocyte-macrophage)	Cytokine	Activated	2.797	1.04E-03	1.236
MAP3K1	Mitogen-activated protein kinase 1, E3 ubiquitin protein ligase	Kinase	Activated	2.802	5.06E-04	
IL18	Interleukin 18 (interferon-gamma-inducing factor)	Cytokine	Activated	2.938	5.40E-02	
TNFRSF1A	Tumour necrosis factor receptor superfamily, member 1A	Transmembrane receptor	Activated	2.956	4.40E-02	
NFkB (complex)	Nuclear factor of kappa light polypeptide gene enhancer in B-cells	Complex	Activated	3.064	1.50E-02	
FOXO1	Forkhead box O1	Transcription regulator	Activated	3.278	9.93E-13	-1.419
TNF	Tumour necrosis factor	Cytokine	Activated	3.842	1.78E-06	
MYD88	Myeloid differentiation primary response gene (88)	Other	Activated	3.857	3.54E-03	
IL1A	Interleukin 1, alpha	Cytokine	Activated	4.315	9.91E-05	
IFNG	Interferon, gamma	Cytokine	Activated	4.527	2.64E-02	

The upstream regulator abbreviation, its description, type of molecule, predicted activation state (activated or inhibited), bias-corrected z-score, p-value and are shown. Also, if the upstream regulator is significantly regulated at the gene expression level in our gene expression dataset, fold changes are depicted. Upstream regulators with an unbiased z-score >2 or < -2, and significant p-value <0.01 are depicted.

that mRNA levels of PGC1α and PGC1β were both significantly downregulated in Fibulin-$4^{R/R}$ compared to Fibulin-$4^{+/+}$ aortas (*Figure 6A*, $P < 0.05$, $n = 11$, and $n = 7$, respectively), whereas levels of PPARα and PPARγ were lower but not significantly different from Fibulin-$4^{+/+}$ (Supplementary material online, *Figure S4C*). Interestingly, in the liver we found that PGC1α was significantly upregulated (Supplementary material online, *Figure S4D*, $P < 0.05$), which would be consistent with the observed lower lipid content (higher lipid usage) of the liver (*Figure 5F*) and the somewhat higher OCR (*Figure 3G*). PGC1α is the master switch between mitochondrial biogenesis and organismal metabolism, and signals to PPARs, essential regulators of lipid metabolism, making these interesting molecules for further investigation. Moreover, when examining the networks predicted to be significantly regulated in our gene expression dataset, the highest significantly regulated network is 'Energy Production/Lipid Metabolism/Small Molecule Biochemistry' (Supplementary material online, *Figure S3*). The visual representation of this network, derived from IPA, highlights that PPARα and PPARγ play a central role (Supplementary material online, *Figure S6A*).

Next, we performed a gene to protein comparison, where we compared the lists of significantly regulated genes and proteins in adult Fibulin-$4^{R/R}$ aortas to Fibulin-$4^{+/+}$. This comparison revealed 30 molecules that changed both at the gene and protein level (Supplementary material online, *Figure S6B*). This list included key genes/proteins involved in metabolism, like glucose-6-phosphate dehydrogenase and fatty acid synthase (Supplementary material online, *Figure S6B*). Strikingly, when we asked whether IPA could find a connection between the 30 overlapping molecules (core analysis on the 30 genes/proteins in common), we indeed found the highest network regulated to be Lipid Metabolism, in which again PPARα and PGC1α are involved as key regulators (Supplementary material online, *Figure S6C*).

In order to check PGC1α activity in VSMCs, we used a luciferase-based assay. We transfected plasmids containing firefly luciferase under the control of the PGC1α promoter in Fibulin-$4^{R/R}$ and Fibulin-$4^{+/+}$ VSMCs, with plasmids containing renilla luciferase as transfection control. Relative luciferase levels, a measure for PGC1α activity, were significantly lower in Fibulin-$4^{R/R}$ VSMCs (*Figure 6B*, $P < 0.01$). It was reported that TGFβ signalling negatively regulates PGC1α.[33,34] As we previously found TGFβ signalling to be increased in Fibulin-$4^{R/R}$ aortas and cells,[13,31] we next investigated the effect of TGFβ signalling on PGC1α. We performed the PGC1α luciferase-based assay on Fibulin-$4^{+/+}$ and Fibulin-$4^{R/R}$ VSMCs with either TGFβ treatment, TGFβR inhibition (SB431542), or Forskolin, a potent inducer of PGC1α activity. In both Fibulin-$4^{+/+}$ and Fibulin-$4^{R/R}$ VSMCs, treatment with TGFβ significantly reduced PGC1α transcription (*Figure 6C*, $P < 0.01$), showing that also in VSMCs TGFβ signalling negatively regulates PGC1α. Yet, TGFβR inhibition did not significantly increase PGC1α activation, pointing to the involvement of non-canonical TGFβ signalling as SB431542 does not inhibit JNK, p38MAPK, or ERK signalling. Forskolin significantly induced PGC1α activity in both Fibulin-$4^{R/R}$ and Fibulin-$4^{+/+}$ VSMCs (*Figure 6C*, $P < 0.01$); in both cases a three-fold induction compared to the untreated situation. These data point to an active inhibition of PGC1α activity in VSMCs of Fibulin-$4^{R/R}$ aortas. We next performed seahorse experiments in which we either examined the effect of TGFβR inhibition, or PGC1α activation. Interestingly, activation of PGC1α increased basal and maximum oxygen consumption in both Fibulin-$4^{+/+}$ and Fibulin-$4^{R/R}$ VSMCs (*Figure 6D*, $P < 0.05$), whereas TGFβR inhibition did not have the same effect. It was previously found that Fibulin-$4^{R/R}$ VSMCs show low proliferation rates compared to Fibulin-$4^{+/+}$ VSMCs, which can be rescued by inhibiting TGFβ.[31] As TGFβ negatively regulates PGC1α levels, we examined whether increased PGC1α levels would also rescue this low proliferation rate. Indeed, PGC1α activation was able to significantly increase the proliferation rate of Fibulin-$4^{R/R}$ VSMCs specifically (*Figure 6E*, $P < 0.01$). Taken together, these results show that PGC1α, an important molecular switch between mitochondrial biogenesis and organismal metabolism, is downregulated in aortas of Fibulin-$4^{R/R}$ animals due to increased TGFβ

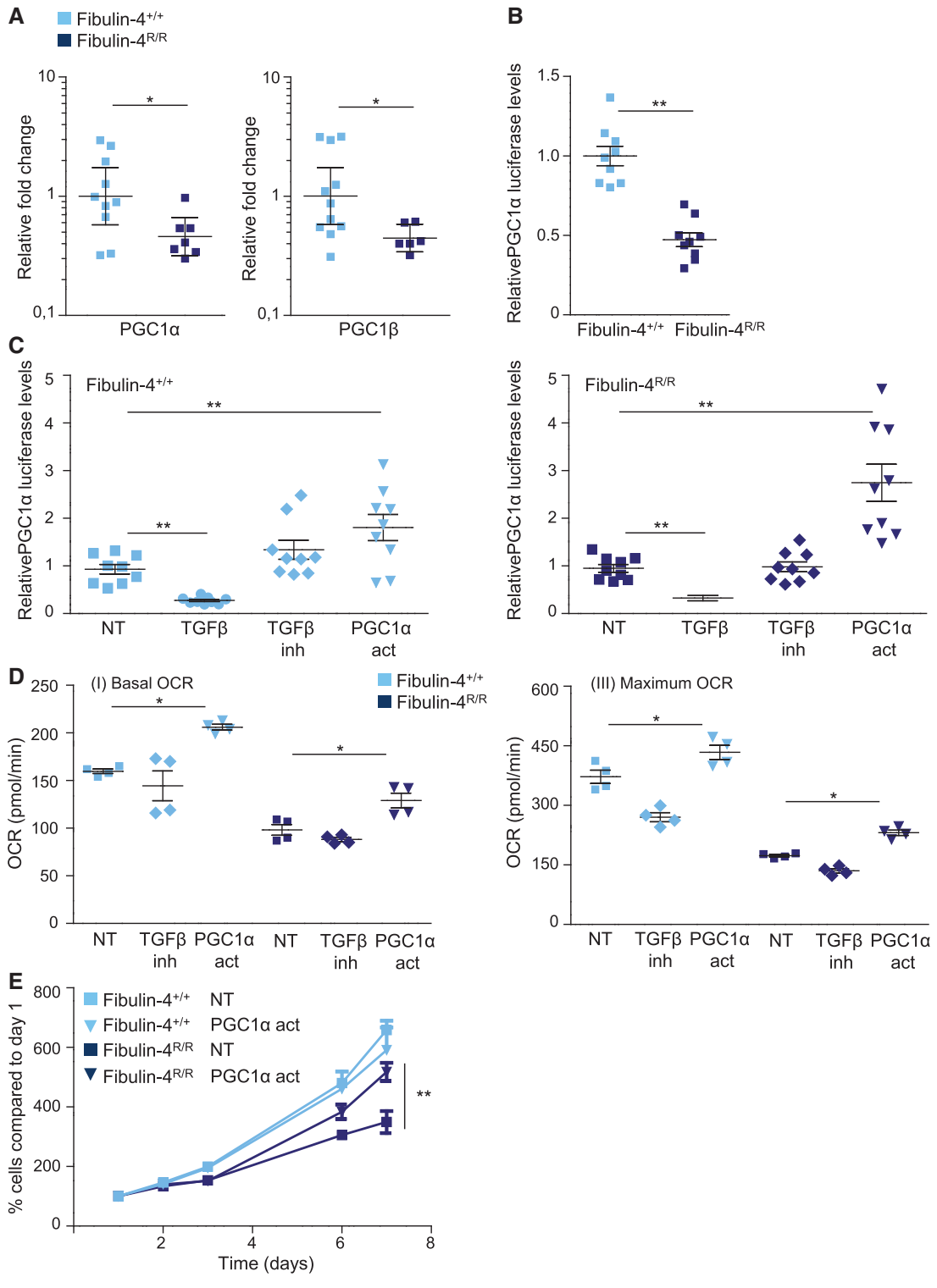

Figure 6 PGC1α expression and activity changes in Fibulin-4$^{R/R}$ aortas and VSMCs. Real-time PCR analysis shows significantly downregulated mRNA levels of PGC1α and PGC1β in Fibulin-4$^{R/R}$ compared to Fibulin-4$^{+/+}$ aortas ($P < 0.05$, $n = 7$, and $n = 11$, respectively, Student's *t*-test on log-transformed data). (*B*) Relative luciferase levels show decreased PGC1α transcriptional activation in Fibulin-4$^{R/R}$ compared to Fibulin-4$^{+/+}$ VSMCs ($P < 0.01$, Student's *t*-test on log-transformed data). (*C*) Relative luciferase levels show decreased PGC1α transcriptional activation after TGFβ treatment in both Fibulin-4$^{R/R}$ (right) and Fibulin-4$^{+/+}$ (left) VSMCs compared to the untreated (NT) control. Forskolin, a potent PGC1α activator, significantly increases PGC1α transcriptional activation in both Fibulin-4$^{R/R}$ and Fibulin-4$^{+/+}$ VSMCs to the same extent as compared to the untreated control. Data are shown for three independent experiments, $n = 3$ cell lines per genotype. TGFβ inhibition does not significantly increase PGC1α activity. (*D*) Scatter plots depicting the basal and maximum oxygen consumption rate (OCR) in Fibulin-4$^{+/+}$ and Fibulin-4$^{R/R}$ VSMCs after Forskolin treatment, which activates PGC1α, compared to the untreated

signalling. When activated, PGC1α can restore the decrease in oxygen consumption and the decreased proliferation in Fibulin-$4^{R/R}$ VSMCs.

4. Discussion

In this study, we took an integrative approach to better understand the molecular mechanisms involved in aneurysm formation, by using a combination of proteomics, genomics and functional experiments on thoracic aortas of aneurysmal Fibulin-$4^{R/R}$ animals. Interestingly, these data indicated changes in mitochondrial function and energy metabolism. Indeed, we measured a decrease in OXPHOS in VSMCs derived from the thoracic aorta of Fibulin-$4^{R/R}$ and Fibulin-$4^{+/+}$ animals. In addition, we observed smaller mitochondria, but not less mitochondria or lower activity of mitochondrial complexes. Furthermore, in Fibulin-$4^{R/R}$ compared to Fibulin-$4^{+/+}$ mice, we observed aortic gene expression differences that indicated altered aortic metabolic processes. Upstream regulator analysis on gene and protein expression data indicated PGC1α, PPARα, and PPARγ as significant regulators in this process. Moreover, we found that PGC1α transcriptional activation was greatly reduced in VSMCs derived from Fibulin-$4^{R/R}$ aortas, and once PGC1α was activated in these VSMCs, this restored the decreased OCR observed in Fibulin-$4^{R/R}$ VSMCs as well as their reduced growth rate.

We verified that the observed defect in mitochondrial function was due to reduced Fibulin-4 in Fibulin-$4^{R/R}$ cells, rather than potential secondary effects associated with the engineered allele; to this end, we used the Fibulin-4^{SMKO} mouse model as a control, in which the Fibulin-4 gene is completely knocked out in VSMCs specifically. Indeed, these Fibulin-4^{SMKO} VSMCs showed a diminished OCR, as we observed for Fibulin-$4^{R/R}$ VSMCs, showing that complete deletion of Fibulin-4 has a similar effect on mitochondrial respiration as the Fibulin-4 reduced allele.

Although very little data are available on involvement of mitochondria in aneurysm formation and development, some evidence points in this direction. For example, mutations in *SLC2A10* result in Arterial Tortuosity Syndrome (ATS, OMIM#208050,[35]) a connective tissue disorder characterized by elongation and tortuosity of the major arteries including the aorta. *SLC2A10* encodes for GLUT10, a glucose transporter that transports l-dehydro ascorbic acid (DHA) into mitochondria. The absence of GLUT10 leads to decreased DHA recycling and thus to more oxidative damage. In zebrafish, defects in this gene lead to problems in development of the cardiovascular system in parallel to mitochondrial dysfunction.[36] In line with this notion, we demonstrate that VSMCs from the Tgfbr-$1^{M318R/+}$ mouse, a model for LDS,[28] similarly show reduced OCR. Moreover, we find that Marfan and Loeys-Dietz patient fibroblasts with mutations in the *FBN1, TGFBR2*, and *SMAD3* genes also show reduced OCR. These observations support the concept that altered mitochondrial function plays a role in aneurysmal disease.

An important question is how a deficiency in a protein involved in structural integrity of the ECM can lead to altered mitochondrial function and metabolism. External cues can lead to cytoskeleton rearrangements since the ECM is connected to the cytoskeleton via integrins. Alternatively, ECM disturbances could invoke alterations in mechanotransduction that lead to modifications in the cytoskeleton or maybe even to its disintegration. Mitochondria depend on the cytoskeleton for their motility and proper function (for review see reference [37]). Thus, if the ECM disintegrates, this could lead to cytoskeleton disintegration due to loss of connections. In turn, this could lead to structural or functional defects in mitochondria. In fact, several genes that are components of the cytoskeleton are mutated in aneurysmal disease, exemplifying that the cytoskeleton is an important factor. One example is *ACTA2*, encoding αSMA, which is a major constituent of the contractile apparatus, that when mutated, leads to ascending aortic aneurysms and dissection (AAT6, OMIM##611788[38]). However, although we did observe mitochondrial function changes and a reduction in mitochondrial size, mitochondrial structure and appearance did not seem to be affected. Also, mitochondria are still aligned along the actin cytoskeleton as could be inferred from EM pictures and stainings for actin.

In addition, Fibulin-$4^{R/R}$ mice show increased TGFβ signalling. Notably, several papers recently reported that TGFβ signalling negatively regulates PGC1α levels.[33,34] Interestingly, derived from our omics data, PGC1α, PPARα, and γ were identified as key components in the mitochondrial biogenesis signalling process. PGC1α is a transcriptional co-activator and is expressed in tissues with high oxidative capacity, where it serves important roles in regulation of mitochondrial functional capacity and cellular energy metabolism.[39] Physiological conditions that demand increased mitochondrial energy production, such as exercise and fasting, induce PGC1α activity. Likewise, low PGC1α levels imply reduced mitochondrial function. Accordingly, studies on PGC1α deficient (PGC1$\alpha^{-/-}$) mice have shown that PGC1α is necessary for regulation of mitochondrial function and cellular metabolism.[40] Both mitochondrial volume density and respiratory capacity are reduced in these mice and there is no normal control of body fat mass, which emphasizes the importance of PGC1α in fatty acid β-oxidation. Furthermore, PGC1$\alpha^{-/-}$ mice do not respond normally to increased demands for energy.[40] PGC1α is involved in the mitochondrial oxidation of fatty acids for energy in the cell through direct co-activation of PPARs.[39] Recently it was shown that PGC1α protein expression is also lowered in aortic material isolated from patients with abdominal aneurysms,[41] which indicates that PGC1α expression may play a regulatory role in both thoracic and abdominal aneurysms.[41] Moreover, increasing mitochondrial function via PGC1α activation has a positive effect on aging and longevity.[42,43] Interestingly, we not only found lower PGC1α expression in Fibulin-$4^{R/R}$ thoracic aortas but also PGC1α transcriptional activation itself was down in Fibulin-$4^{R/R}$ VSMCs. However, this activation could be enhanced by Forskolin, a PGC1α activator, and enhancement of PGC1α activation was able to restore the decreased oxidative respiration observed in Fibulin-$4^{R/R}$ VSMCs.

We also found that TGFβ decreased PGC1α transcriptional levels in Fibulin-$4^{+/+}$ and Fibulin-$4^{R/R}$ VSMCs, implying that the increased TGFβ signalling in Fibulin-$4^{R/R}$ aortas and VSMCs is responsible for the decreased PGC1α levels, thus impacting mitochondrial respiration. This

Figure 6 Continued
controls, and TGFβ inhibition. Both Fibulin-$4^{+/+}$ and to Fibulin-$4^{R/R}$ show a significant increase in basal and maximum OCR compared to the untreated controls ($P < 0.01$, Student's *t*-test) after Forskolin treatment. TGFβ inhibition does not show a significant increase. Experiments were performed twice, $n = 2$ cell lines per genotype. (*E*) Growth curves of Fibulin-$4^{R/R}$ and Fibulin-$4^{+/+}$ VSMCs showing that activation of PGC1α significantly restores the reduced growth of Fibulin-$4^{R/R}$ VSMCs compared to the untreated situation (NT) ($P < 0.01$, non-linear fit of exponential decay). Experiments were performed twice, $n = 2$ cell lines per genotype, the mean of two cell lines is shown. All results are expressed as mean ± SEM.

would also explain why we find reduced mitochondrial respiration in cells derived from other aneurysmal syndromes that show increased TGFβ signalling, such as LDS and Marfan. Ramnath *et al.*[31] showed that lowering of TGFβ levels in Fibulin-4$^{R/R}$ VSMCs restored their reduced proliferation rate. Similarly, we now show that by activating PGC1α, we can also increase this proliferation rate, suggesting that this reduced proliferation phenotype is induced by increased TGFβ levels, possibly via PGC1α reduction.

It is evident that mitochondria are major cellular sources of ROS and changes in metabolism can alter mitochondrial function and the resulting ROS production. Likewise, in Fibulin-4$^{R/R}$ animals, we find evidence for increased ROS in the aorta. In this regard, changes in mitochondrial metabolism could also be an attempt to adapt to increased ROS, or to reduce ROS in response to a potential source of damage, at the organismal level. In line with this, we also find reduced oxygen consumption in other muscle cell containing organs; heart and skeletal muscle, but not in kidney or liver. Furthermore, in Fibulin-4$^{R/R}$ animals we observe a relative shift from glucose utilization to fatty acid usage as evidenced from metabolic parameters in blood and liver, as well as from our aortic gene expression analysis. The accumulation of glycogen in the liver might indicate increased storage of glucose into glycogen, in accordance to a relative increase in fatty acid β-oxidation that provides the energy for gluconeogenesis in the absence of an increased demand for glucose from the liver. Interestingly, newborn livers do not yet show these changes in liver metabolism. However, they do already show aneurysms, which may indicate that the aortic structural and/or signalling changes induce the liver metabolic changes at a later stage. The observed metabolic changes in adult Fibulin-4$^{R/R}$ mice are even more interesting since we did not detect changes in the liver mitochondrial complexes themselves, but did observe upregulation of PGC1α mRNA levels, pointing to a normal response of the liver to a change in demand of energy carrier type. Plasma measurements of Fibulin-4$^{R/R}$ mice show significantly lower levels of ketone bodies compared to their wild-type littermates. Taken together, this could indicate that the thoracic aorta of Fibulin-4$^{R/R}$ mice retrieves its energy from ketone bodies rather than from glucose, which could be the underlying reason for the liver to switch from glucose to fatty acid usage. In fact, adapting organismal metabolism under conditions of stress, such as organ damage, is a well-known survival mechanism in aging that attempts to preserve the organism by allowing time and energy for repair.[44,45] Actually, mitochondrial dysfunction itself is considered an important hallmark of aging.[46] ROS and mitochondrial dysfunction both increase with age, resulting in decreased bioenergetic efficiency. In fact, age-related aneurysms show many vascular aging characteristics such as elastin breakdown, collagen deposition as well as morphological changes in VSMCs.[47] Previously, we identified similar overexpression of miR-29b in Fibulin-4$^{R/R}$ aneurysmal aortas and aging mouse aortas, concomitant with reduced ECM protein expression thereby sensitizing the aorta for aneurysms formation.[32] In line with this, structural ECM changes could induce signalling processes that are partly mediated by TGFβ, including those involving mitochondrial biogenesis. These signalling responses would then attempt to reduce aortic damage, similar to the organismal response observed in aging.

In this context, it would be interesting to see the effect of PGC1α activators on aneurysm formation in the Fibulin-4$^{R/R}$ mouse. Previously, calorie restriction has been shown to have positive effects on mitochondrial biogenesis as well as many aging characteristics in different species[48,49] and notably also affects PGC1α signalling by increasing PGC1α. In line with this, the results reported here could open up the exciting possibility of nutritional interventions as a possible treatment for aneurysmal disease.

Supplementary material

Supplementary material is available at *Cardiovascular Research* online.

Acknowledgements

We would like to thank Julian Benschop for isolating the RNA used in the gene expression experiments, Bibi van Thiel, Susan Ghazi, and Sylvia Gabriëls for technical assistance, Daniëlle Majoor-Krakauer, Ingrid van der Laar, and Judith Verhagen for providing the human patient fibroblasts, Carmen Halabi for providing us with the Fibulin-4 antibody, and the Biomics core facility at the Erasmus Medical Center for running the mouse exon arrays. We acknowledge Bruce Spiegelman for the use of the Addgene plasmid 8887 in the PGC1α luciferase assay.

Conflict of interest: none declared.

Funding

This work was supported by the 'Lijf en Leven' grant (2011) 'DIVERS' (dilaterend versus stenoserend vaatlijden) and the 'Lijf and Leven' grant (2014) "GAMMA" (Genexpressie analyse ter detectie van de moleculaire mechanismen van aneurysmavorming) (J.B.) (I.v.d.P., P.v.H., and J.E.); The FACS machine was purchased thanks to the ZonMW (91109036) equipment grant (R.v.d.L.).

References

1. Longo GM, Xiong W, Greiner TC, Zhao Y, Fiotti N, Baxter BT. Matrix metalloproteinases 2 and 9 work in concert to produce aortic aneurysms. *J Clin Invest* 2002;**110**:625–632.
2. Neptune ER, Frischmeyer PA, Arking DE, Myers L, Bunton TE, Gayraud B, Ramirez F, Sakai LY, Dietz HC. Dysregulation of TGF-beta activation contributes to pathogenesis in Marfan syndrome. *Nat Genet* 2003;**33**:407–411.
3. Loeys BL, Chen J, Neptune ER, Judge DP, Podowski M, Holm T, Meyers J, Leitch CC, Katsanis N, Sharifi N, Xu FL, Myers LA, Spevak PJ, Cameron DE, De Backer J, Hellemans J, Chen Y, Davis EC, Webb CL, Kress W, Coucke P, Rifkin DB, De Paepe AM, Dietz HC. A syndrome of altered cardiovascular, craniofacial, neurocognitive and skeletal development caused by mutations in TGFBR1 or TGFBR2. *Nat Genet* 2005;**37**:275–281.
4. Moltzer E, Essers J, van Esch JH, Roos-Hesselink JW, Danser AH. The role of the renin-angiotensin system in thoracic aortic aneurysms: clinical implications. *Pharmacol Ther* 2011;**131**:50–60.
5. Moltzer E, Te Riet L, Swagemakers SM, van Heijningen PM, Vermeij M, van Veghel R, Bouhuizen AM, van Esch JH, Lankhorst S, Ramnath NW, de Waard MC, Duncker DJ, van der Spek PJ, Rouwet EV, Danser AH, Essers J. Impaired vascular contractility and aortic wall degeneration in fibulin-4 deficient mice: effect of angiotensin II type 1 (AT1) receptor blockade. *PLoS One* 2011;**6**:e23411.
6. Holm TM, Habashi JP, Doyle JJ, Bedja D, Chen Y, van Erp C, Lindsay ME, Kim D, Schoenhoff F, Cohn RD, Loeys BL, Thomas CJ, Patnaik S, Marugan JJ, Judge DP, Dietz HC. Noncanonical TGFbeta signaling contributes to aortic aneurysm progression in Marfan syndrome mice. *Science* 2011;**332**:358–361.
7. Huang J, Yamashiro Y, Papke CL, Ikeda Y, Lin Y, Patel M, Inagami T, Le VP, Wagenseil JE, Yanagisawa H. Angiotensin-converting enzyme-induced activation of local angiotensin signaling is required for ascending aortic aneurysms in fibulin-4-deficient mice. *Sci Transl Med* 2013;**5**:183ra58.
8. Cook JR, Carta L, Galatioto J, Ramirez F. Cardiovascular manifestations in Marfan syndrome and related diseases: multiple genes causing similar phenotypes. *Clin Genet* 2015;**87**:11–20.
9. Yamashiro Y, Yanagisawa H . Crossing bridges between extra- and intra-cellular events in thoracic aortic aneurysms. *J Atheroscler Thromb* 2018;**25**:99–110.
10. Brooke BS, Habashi JP, Judge DP, Patel N, Loeys B, Dietz HC. Angiotensin II blockade and aortic-root dilation in Marfan's syndrome. *N Engl J Med* 2008;**358**:2787–2795.
11. Habashi JP, Doyle JJ, Holm TM, Aziz H, Schoenhoff F, Bedja D, Chen Y, Modiri AN, Judge DP, Dietz HC. Angiotensin II type 2 receptor signaling attenuates aortic aneurysm in mice through ERK antagonism. *Science* 2011;**332**:361–365.
12. Habashi JP, Judge DP, Holm TM, Cohn RD, Loeys BL, Cooper TK, Myers L, Klein EC, Liu G, Calvi C, Podowski M, Neptune ER, Halushka MK, Bedja D, Gabrielson K, Rifkin DB, Carta L, Ramirez F, Huso DL, Dietz HC. Losartan, an AT1 antagonist, prevents aortic aneurysm in a mouse model of Marfan syndrome. *Science* 2006;**312**:117–121.

13. Hanada K, Vermeij M, Garinis GA, de Waard MC, Kunen MG, Myers L, Maas A, Duncker DJ, Meijers C, Dietz HC, Kanaar R, Essers J. Perturbations of vascular homeostasis and aortic valve abnormalities in fibulin-4 deficient mice. *Circ Res* 2007;**100**: 738–746.
14. Kaijzel EL, van Heijningen PM, Wielopolski PA, Vermeij M, Koning GA, van Cappellen WA, Que I, Chan A, Dijkstra J, Ramnath NW, Hawinkels LJ, Bernsen MR, Lowik CW, Essers J. Multimodality imaging reveals a gradual increase in matrix metalloproteinase activity at aneurysmal lesions in live fibulin-4 mice. *Circ Cardiovasc Imaging* 2010;**3**:567–577.
15. Ramnath NW, van de Luijtgaarden KM, van der Pluijm I, van Nimwegen M, van Heijningen PM, Swagemakers SM, van Thiel BS, Ridwan RY, van Vliet N, Vermeij M, Hawinkels LJ, de Munck A, Dzyubachyk O, Meijering E, van der Spek P, Rottier R, Yanagisawa H, Hendriks RW, Kanaar R, Rouwet EV, Kleinjan A, Essers J. Extracellular matrix defects in aneurysmal fibulin-4 mice predispose to lung emphysema. *PLoS One* 2014;**9**:e106054.
16. Argraves WS, Greene LM, Cooley MA, Gallagher WM. Fibulins: physiological and disease perspectives. *EMBO Rep* 2003;**4**:1127–1131.
17. Chen Q, Zhang T, Roshetsky JF, Ouyang Z, Essers J, Fan C, Wang Q, Hinek A, Plow EF, Dicorleto PE. Fibulin-4 regulates expression of the tropoelastin gene and consequent elastic-fibre formation by human fibroblasts. *Biochem J* 2009;**423**:79–89.
18. Giltay R, Timpl R, Kostka G. Sequence, recombinant expression and tissue localization of two novel extracellular matrix proteins, fibulin-3 and fibulin-4. *Matrix Biol* 1999;**18**:469–480.
19. Davis EC. Smooth muscle cell to elastic lamina connections in developing mouse aorta. Role in aortic medial organization. *Lab Invest* 1993;**68**:89–99.
20. Dasouki M, Markova D, Garola R, Sasaki T, Charbonneau NL, Sakai LY, Chu ML. Compound heterozygous mutations in fibulin-4 causing neonatal lethal pulmonary artery occlusion, aortic aneurysm, arachnodactyly, and mild cutis laxa. *Am J Med Genet* 2007;**143A**:2635–2641.
21. Hoyer J, Kraus C, Hammersen G, Geppert JP, Rauch A. Lethal cutis laxa with contractural arachnodactyly, overgrowth and soft tissue bleeding due to a novel homozygous fibulin-4 gene mutation. *Clin Genet* 2009;**76**:276–281.
22. Renard M, Holm T, Veith R, Callewaert BL, Ades LC, Baspinar O, Pickart A, Dasouki M, Hoyer J, Rauch A, Trapane P, Earing MG, Coucke PJ, Sakai LY, Dietz HC, De Paepe AM, Loeys BL. Altered TGFbeta signaling and cardiovascular manifestations in patients with autosomal recessive cutis laxa type I caused by fibulin-4 deficiency. *Eur J Hum Genet* 2010;**18**:895–901.
23. McLaughlin PJ, Chen Q, Horiguchi M, Starcher BC, Stanton JB, Broekelmann TJ, Marmorstein AD, McKay B, Mecham R, Nakamura T, Marmorstein LY. Targeted disruption of fibulin-4 abolishes elastogenesis and causes perinatal lethality in mice. *Mol Cell Biol* 2006;**26**:1700–1709.
24. Huang J, Davis EC, Chapman SL, Budatha M, Marmorstein LY, Word RA, Yanagisawa H. Fibulin-4 deficiency results in ascending aortic aneurysms: a potential link between abnormal smooth muscle cell phenotype and aneurysm progression. *Circ Res* 2010; **106**:583–592.
25. Cox B, Emili A. Tissue subcellular fractionation and protein extraction for use in mass-spectrometry-based proteomics. *Nat Protoc* 2006;**1**:1872–1878.
26. van den Berg DL, Snoek T, Mullin NP, Yates A, Bezstarosti K, Demmers J, Chambers I, Poot RA. An Oct4-centered protein interaction network in embryonic stem cells. *Cell Stem Cell* 2010;**6**:369–381.
27. Proudfoot D, Shanahan C. Human vascular smooth muscle cell culture. In RR Mitry, RD Hughes (eds). *Human Cell Culture Protocols (Methods in Molecular Biology)*. Vol 806. Humana Press, Switzerland AG: Springer, 2012. pp. 251–63.
28. Gallo EM, Loch DC, Habashi JP, Calderon JF, Chen Y, Bedja D, van Erp C, Gerber EE, Parker SJ, Sauls K, Judge DP, Cooke SK, Lindsay ME, Rouf R, Myers L, Ap Rhys CM, Kent KC, Norris RA, Huso DL, Dietz HC. Angiotensin II-dependent TGF-beta signaling contributes to Loeys-Dietz syndrome vascular pathogenesis. *J Clin Invest* 2014;**124**:448–460.
29. Kielland A, Blom T, Nandakumar KS, Holmdahl R, Blomhoff R, Carlsen H. In vivo imaging of reactive oxygen and nitrogen species in inflammation using the luminescent probe L-012. *Free Radic Biol Med* 2009;**47**:760–766.
30. Handschin C, Rhee J, Lin J, Tarr PT, Spiegelman BM. An autoregulatory loop controls peroxisome proliferator-activated receptor gamma coactivator 1alpha expression in muscle. *Proc Natl Acad Sci USA* 2003;**100**:7111–7116.
31. Ramnath NW, Hawinkels LJ, van Heijningen PM, Riet LT, Paauwe M, Vermeij M, Danser AH, Kanaar R, Ten Dijke P, Essers J. Fibulin-4 deficiency increases TGF-beta signalling in aortic smooth muscle cells due to elevated TGF-beta2 levels. *Sci Rep* 2015;**5**:16872.
32. Boon RA, Seeger T, Heydt S, Fischer A, Hergenreider E, Horrevoets AJ, Vinciguerra M, Rosenthal N, Sciacca S, Pilato M, van Heijningen P, Essers J, Brandes RP, Zeiher AM, Dimmeler S. MicroRNA-29 in aortic dilation: implications for aneurysm formation. *Circ Res* 2011;**109**:1115–1119.
33. Tiano JP, Springer DA, Rane SG. SMAD3 negatively regulates serum irisin and skeletal muscle FNDC5 and peroxisome proliferator-activated receptor gamma coactivator 1-alpha (PGC-1alpha) during exercise. *J Biol Chem* 2015;**290**:11431.
34. Yadav H, Quijano C, Kamaraju AK, Gavrilova O, Malek R, Chen W, Zerfas P, Zhigang D, Wright EC, Stuelten C, Sun P, Lonning S, Skarulis M, Sumner AE, Finkel T, Rane SG. Protection from obesity and diabetes by blockade of TGF-beta/Smad3 signaling. *Cell Metab* 2011;**14**:67–79.
35. Coucke PJ, Willaert A, Wessels MW, Callewaert B, Zoppi N, De Backer J, Fox JE, Mancini GM, Kambouris M, Gardella R, Facchetti F, Willems PJ, Forsyth R, Dietz HC, Barlati S, Colombi M, Loeys B, De Paepe A. Mutations in the facilitative glucose transporter GLUT10 alter angiogenesis and cause arterial tortuosity syndrome. *Nat Genet* 2006;**38**:452–457.
36. Willaert A, Khatri S, Callewaert BL, Coucke PJ, Crosby SD, Lee JG, Davis EC, Shiva S, Tsang M, De Paepe A, Urban Z. GLUT10 is required for the development of the cardiovascular system and the notochord and connects mitochondrial function to TGFbeta signaling. *Hum Mol Genet* 2012;**21**:1248–1259.
37. de Cavanagh EM, Ferder M, Inserra F, Ferder L. Angiotensin II, mitochondria, cytoskeletal, and extracellular matrix connections: an integrating viewpoint. *Am J Physiol Heart Circ Physiol* 2009;**296**:H550–H558.
38. Guo DC, Pannu H, Tran-Fadulu V, Papke CL, Yu RK, Avidan N, Bourgeois S, Estrera AL, Safi HJ, Sparks E, Amor D, Ades L, McConnell V, Willoughby CE, Abuelo D, Willing M, Lewis RA, Kim DH, Scherer S, Tung PP, Ahn C, Buja LM, Raman CS, Shete SS, Milewicz DM. Mutations in smooth muscle alpha-actin (ACTA2) lead to thoracic aortic aneurysms and dissections. *Nat Genet* 2007;**39**:1488–1493.
39. Finck BN, Kelly DP. PGC-1 coactivators: inducible regulators of energy metabolism in health and disease. *J Clin Invest* 2006;**116**:615–622.
40. Leone TC, Lehman JJ, Finck BN, Schaeffer PJ, Wende AR, Boudina S, Courtois M, Wozniak DF, Sambandam N, Bernal-Mizrachi C, Chen Z, Holloszy JO, Medeiros DM, Schmidt RE, Saffitz JE, Abel ED, Semenkovich CF, Kelly DP. PGC-1alpha deficiency causes multi-system energy metabolic derangements: muscle dysfunction, abnormal weight control and hepatic steatosis. *PLoS Biol* 2005;**3**:e101.
41. Gabrielson M, Vorkapic E, Folkesson M, Welander M, Matussek A, Dimberg J, Länne T, Skogberg J, Wågsäter D. Wagsater D. Altered PPARgamma coactivator-1 alpha expression in abdominal aortic aneurysm: possible effects on mitochondrial biogenesis. *J Vasc Res* 2016;**53**:17–26.
42. Feige JN, Lagouge M, Canto C, Strehle A, Houten SM, Milne JC, Lambert PD, Mataki C, Elliott PJ, Auwerx J. Specific SIRT1 activation mimics low energy levels and protects against diet-induced metabolic disorders by enhancing fat oxidation. *Cell Metab* 2008;**8**:347–358.
43. Rera M, Bahadorani S, Cho J, Koehler CL, Ulgherait M, Hur JH, Ansari WS, Lo T Jr, Jones DL, Walker DW. Modulation of longevity and tissue homeostasis by the *Drosophila* PGC-1 homolog. *Cell Metab* 2011;**14**:623–634.
44. Schumacher B, van der Pluijm I, Moorhouse MJ, Kosteas T, Robinson AR, Suh Y, Breit TM, van Steeg H, Niedernhofer LJ, van Ijcken W, Bartke A, Spindler SR, Hoeijmakers JH, van der Horst GT, Garinis GA. Delayed and accelerated aging share common longevity assurance mechanisms. *PLoS Genet* 2008;**4**:e1000161.
45. van der Pluijm I, Garinis GA, Brandt RM, Gorgels TG, Wijnhoven SW, Diderich KE, de Wit J, Mitchell JR, van Oostrom C, Beems R, Niedernhofer LJ, Velasco S, Friedberg EC, Tanaka K, van Steeg H, Hoeijmakers JH, van der Horst GT. Impaired genome maintenance suppresses the growth hormone–insulin-like growth factor 1 axis in mice with Cockayne syndrome. *PLoS Biol* 2006;**5**:e2.
46. Lopez-Otin C, Blasco MA, Partridge L, Serrano M, Kroemer G. The hallmarks of aging. *Cell* 2013;**153**:1194–1217.
47. Collins JA, Munoz JV, Patel TR, Loukas M, Tubbs RS. The anatomy of the aging aorta. *Clin Anat* 2014;**27**:463–466.
48. Colman RJ, Anderson RM, Johnson SC, Kastman EK, Kosmatka KJ, Beasley TM, Allison DB, Cruzen C, Simmons HA, Kemnitz JW, Weindruch R. Caloric restriction delays disease onset and mortality in rhesus monkeys. *Science* 2009;**325**:201–204.
49. Vermeij WP, Dolle ME, Reiling E, Jaarsma D, Payan-Gomez C, Bombardieri CR, Wu H, Roks AJ, Botter SM, van der Eerden BC, Youssef SA, Kuiper RV, Nagarajah B, van Oostrom CT, Brandt RM, Barnhoorn S, Imholz S, Pennings JL, de Bruin A, Gyenis A, Pothof J, Vijg J, van Steeg H, Hoeijmakers JH. Restricted diet delays accelerated ageing and genomic stress in DNA-repair-deficient mice. *Nature* 2016;**537**:427–431.